Geomorphology 379 (2021) 107548

Contents lists available at ScienceDirect

Geomorphology

journal homepage: www.elsevier.com/locate/geomorph

Mesophotic reef geomorphology categorization, habitat identification, and relationships with surface cover and terrace formation in the Gulf of Aqaba

David K. Weinstein [a,b,*], Raz Tamir [b,c], Netanel Kramer [c], Gal Eyal [d,e], Igal Berenshtein [f], Yonathan Shaked [b], Yossi Loya [c], Adi Torfstein [a,b]

[a] The Fredy & Nadine Herrmann Institute of Earth Sciences, The Hebrew University of Jerusalem, Jerusalem, Israel
[b] Interuniversity Institute for Marine Sciences, Eilat, Israel
[c] School of Zoology, Tel-Aviv University, Tel Aviv, Israel
[d] ARC Centre of Excellence for Coral Reef Studies, School of Biological Sciences, The University of Queensland, QLD, Australia
[e] The Mina & Everard Goodman Faculty of Life Sciences, Bar Ilan University, Ramat Gan, Israel
[f] Department of Ocean Sciences, Rosenstiel School of Marine and Atmospheric Science, University of Miami, Miami, FL, United States

ARTICLE INFO

Article history:
Received 22 April 2020
Received in revised form 17 November 2020
Accepted 25 November 2020
Available online 2 December 2020

Keywords:
Mesophotic coral ecosystems (MCEs)
Red Sea
Benthic cover
Reef lithology
Coral rubble
Bathymetry

ABSTRACT

Antecedent topography such as relic reef terraces as well as biogenic carbonate relief-forming deposits ~30–150 m deep, referred to as mesophotic reefs, provide structural support for diverse mesophotic coral ecosystems (MCEs) that may serve as coral refuges for select light-dependent species. Although terraces at mesophotic depths are found globally, an understanding of their spatial distribution, formation, and relationship with living community composition and lithology is generally lacking. Herein, 2 × 2 m resolution bathymetry from the Gulf of Aqaba (GoA) was examined to define geomorphology features spanning mesophotic depths and compare geomorphology relationships to overlying benthic and lithologic cover. Analysis led to the production of a new map categorizing 12 geomorphology features, including upper mesophotic terraces harboring thriving MCEs. Additionally, a large collection of still imagery (1726 pictures) was obtained at 94 sites and used to define eight unique habitats at mesophotic depths and lithological and biological distribution patterns over vertical and horizontal scales. Study area benthic and lithologic cover was found to be significantly different between geomorphology features and related to GoA geomorphology as well as to seafloor depth and slope, and light attenuation. While these relationships indicated modern cover could not provide a model for producing most underlying geomorphology in the study area, results provided data needed to enhance understanding of geomorphology feature formation history and reef accretion at mesophotic depths. Study results also detailed benthic cover and geomorphology features critical for better identifying and mapping unknown MCE habitats, and for recognizing mesophotic reef spatial relationships and biodiversity patterns in the GoA. These results are especially important considering most northern GoA reefs act as potential refuges, but local anthropogenic development continually stresses shallow GoA reefs and most other shallow coral reefs around the globe continue to degrade.

1. Introduction

As shallow coral reefs continue to decline worldwide (Pandolfi et al., 2003; Hughes et al., 2018), the identification, mapping, and management of reef refuges become increasingly important (Riegl and Piller, 2003; Cacciapaglia and van Woesik, 2015). Communities of light-dependent corals and associated organisms at dim ocean depths between ~30–150 m, now termed mesophotic coral ecosystems (MCEs; Hinderstein et al., 2010), were initially hypothesized to act as refugia given their relative shelter from environmental and anthropogenic stressors and temperature fluctuations (Riegl and Piller, 2003; Lesser et al., 2009; Bongaerts et al., 2010). However, more recent studies have questioned this hypothesis (Bongaerts et al., 2017; Rocha et al., 2018; Shlesinger et al., 2018) and the potential protection afforded to MCEs, at least at upper mesophotic depth boundaries ~30–60 m, from major disturbances (Lesser and Slattery, 2011; White et al., 2017; Frade et al., 2018). Still, there is likely some degree of connectivity between MCEs and shallower coral reefs on a limited and species-specific scope and mesophotic depths offer some level of protection from disturbance (e.g. Bongaerts et al., 2017; Frade et al., 2018). Many coral species live both at shallow and mesophotic depths. In the western Atlantic Ocean, 85% of total coral species found in the mesophotic zone are shallow reef species while 45% have this distinction in the Indo-

* Corresponding author:
E-mail address: dweinstein@rsmas.miami.edu (D.K. Weinstein).

https://doi.org/10.1016/j.geomorph.2020.107548
0169-555X/

Pacific (Muir and Pichon, 2019). Furthermore, although the potential for low-latitude coral species to migrate to higher latitudes in the recurrent global warming crisis is limited by winter photosynthetically available radiation (Muir et al., 2015), large abundances of species and high diversity have recently been found on many high-latitude MCEs (see examples from Loya et al., 2019).

The Gulf of Aqaba (GoA), constituting a relatively shallow (900 m average depth) ~53 km^2 area northeast extension of the Red Sea, borders Israel, Egypt, Jordan, and Saudi Arabia at a latitude spanning ~27°99′N to 29°54′N. Residing in a semi-enclosed arid basin with high relative salinity (~40.5 ppt) and warm water (21–30 °C and 21–28 °C at 10 m and 50 m depths, respectively; Eyal et al., 2019), reefs found along the GoA coastline represent one of the highest latitude coral ecosystems in the Indo-Pacific region (Loya, 1972). Modern GoA reefs were previously characterized by high coral species diversity peaking around 30 m deep and coral cover was identified as greater on steeper than flatter zones (Loya, 1972). Hermatypic corals are also found at lower mesophotic depths (60–150 m); *Leptoseris fragilis* was identified as deep as 145 m (Fricke et al., 1987). Production rates of habitat-forming topographic relief during the late Holocene, in terms of vertical accretion, have been estimated between 0.67 and 1.5 m/kyr for shallow water Red Sea reefs (Dullo et al., 1996; Purkis et al., 2010) but no rates are currently available at deeper depths. Still, previous studies have characterized GoA submarine terraces and lineaments at depths 50–120 m (Reches et al., 1987; Makovsky et al., 2008; Tibor et al., 2010), some of which are known to host modern MCEs (Eyal et al., 2019).

Mesophotic reefs, herein defined as suspected biogenic carbonate structures with topographic relief at mesophotic depths, are uniquely positioned in the GoA to function as prevailing regional coral habitats (Eyal et al., 2019). This stems from the thriving health of associated coral at deep depths and high latitude (Eyal et al., 2019), potential vertical connectivity (Berenshtein et al., 2016), and residence in a region where corals have a high thermal tolerance potentially from past natural selection through a thermal barrier (see Fine et al., 2013). Extending no further than 2 km from shore, the potential spatial extent of northern GoA mesophotic reefs compared to shallower counterparts is almost double (Eyal et al., 2019). However, confirmation of GoA mesophotic reef distribution and identification of benthic and lithologic spatial patterns and drivers are sparse.

Bathymetric and geomorphologic analysis has shown promise predicting mesophotic reef distribution and benthic cover (e.g. Bridge et al., 2012; Costa et al., 2015; Linklater et al., 2016). In addition, geomorphology is suggested to impose a fundamental regulation on MCE distribution, occurrence, and productivity (Sherman et al., 2019). Mesophotic coral ecosystems often proliferate atop antecedent topography such as relict reefs and may contribute to underlying carbonate accretion (Sherman et al., 2019). As such, studying modern mesophotic reef spatial distribution and associated geomorphology is critical for determining the location of MCEs and the continued production and/or maintenance of complex substrates needed to support them. Despite the high potential of GoA MCEs to function as refuges and their noted relevance in scientific advancement (Loya et al., 2016; Turner et al., 2017), northern GoA seafloor geomorphology and development has not been investigated or classified in detail specifically at mesophotic depths, particularly in relation to benthic and lithologic cover.

The primary objectives of this study were to (1) identify and map GoA geomorphology features spanning mesophotic depths, (2) resolve lithologic and benthic cover variability between geomorphology features and determine which factors related to lithologic and benthic cover at mesophotic depths, and (3) consider newly mapped geomorphology development and timing. Results facilitate the identification of regional MCEs, as well as an understanding of GoA benthic cover characteristics and potential contributions to past and future geomorphology. Characterizing the spatial distribution of geomorphology features and associated benthic cover, and establishing a baseline for ecological productivity at northern GoA mesophotic depths also provides a basis for studies ranging from regional tectonics to future risk assessment of increasing anthropogenic stressors along the GoA (e.g. desalination plants, increased coastal settlement; Fine et al., 2019).

2. Regional settings

The GoA is an ~180 km long, narrow (15–25 km wide) expanse within an active left-lateral strike-slip fault zone at the southern end of the Dead Sea Transform Fault system (Ben-Avraham et al., 1979). The northern GoA is flanked by mountains composed of late Precambrian plutonic and metamorphic rocks and Cretaceous-Eocene sedimentary deposits towering up to 1.5 km above the modern sea level (Ben-Avraham et al., 1979). Exposed Pleistocene and Holocene reefs and terraces are found throughout the region (Braithwaite, 1987; Al-Rifaiy and Cherif, 1988; Klein et al., 1990). Despite little tectonic displacement since sea level stabilized in the late Holocene (Shaked et al., 2002), down-faulting-induced burial attests to more recent limited vertical displacement (Shaked et al., 2011). The northern GoA was previously mapped with a hull-mounted Simrad EM 1002 multibeam sonar system (95 kHz frequency), processed to a 2-m data grid of depth and 2 × 2 resolution (Sade et al., 2008; Tibor et al., 2010). The current study focuses on a seafloor area covering 3.7 km^2 adjacent to the southernmost Israeli border, with a northeastern extent selected to prevent interference with local port operations. The shallowest depths of the mapped area start at ~10 m, depending on bathymetry data coverage. The deepest depths of the study area are found at 150 m, the most commonly accepted definition of lower MCE limits (Hinderstein et al., 2010).

3. Methods

3.1. Geomorphology classification

The existing northern GoA multibeam bathymetry dataset (Sade et al., 2008; Tibor et al., 2010) was examined in ArcMap 10.5 and ArcScene 10.5, projected to the World Geodetic System (WGS) 1984 UTM Zone 36 N (Supplementary Fig. 1a), and used to create hillshade and slope rasters (Fig. 1 and Supplementary Fig. 1b, respectively). Depth, slope, and spatial GoA characteristics were used to identify geomorphology features spanning mesophotic depths without consideration for underlying cover. Therefore, as a precautionary approach, no attempt was made to classify geomorphology features as reefs. To limit manual interpretations with feature division, three GoA-specific depth zones were used. Zone determination was based on three main coral assemblages that regionally differ above the 36 m isobath (yearly averaged 1% ultraviolet radiation), between the 36 m and 76 m isobath, and below the 76 m isobath (yearly averaged 1% photosynthetically active radiation). These isobaths were suggested by Tamir et al. (2019) and Laverick et al. (2020) as the depths where GoA coral communities change following light environmental conditions along the reef slope. As such, some geomorphology features were divided using the following similar reef depth zones: shallow (depth <35 m), upper MCEs (35 m ≥ depth <75 m), and lower MCEs (depth ≥75 m).

The mapped area was initially divided into steep gradients, terraces, shelves, and incised channels with ArcGIS before formal geomorphology features were established. General definitions are provided in Table 1. Steep gradients were divided by the three GoA-specific depth zones into shallow, upper, and lower steep gradient geomorphology features. Terraces (Table 1 definition modified from International Hydrographic Organization (IHO), 2013) were mapped by manually tracing smoothed polygons converted from the slope raster and were classified as a lower mesophotic terrace (LMT) when part of a polygon meeting terrace criteria was found in water ≥75 m deep, or as an upper mesophotic terrace (UMT). Southernmost terrace identification was based on previous knowledge that an ~12–40 m deep steep gradient continues southward and examination of low-resolution shallow-water bathymetry (Israeli government agency for mapping, geodesy,

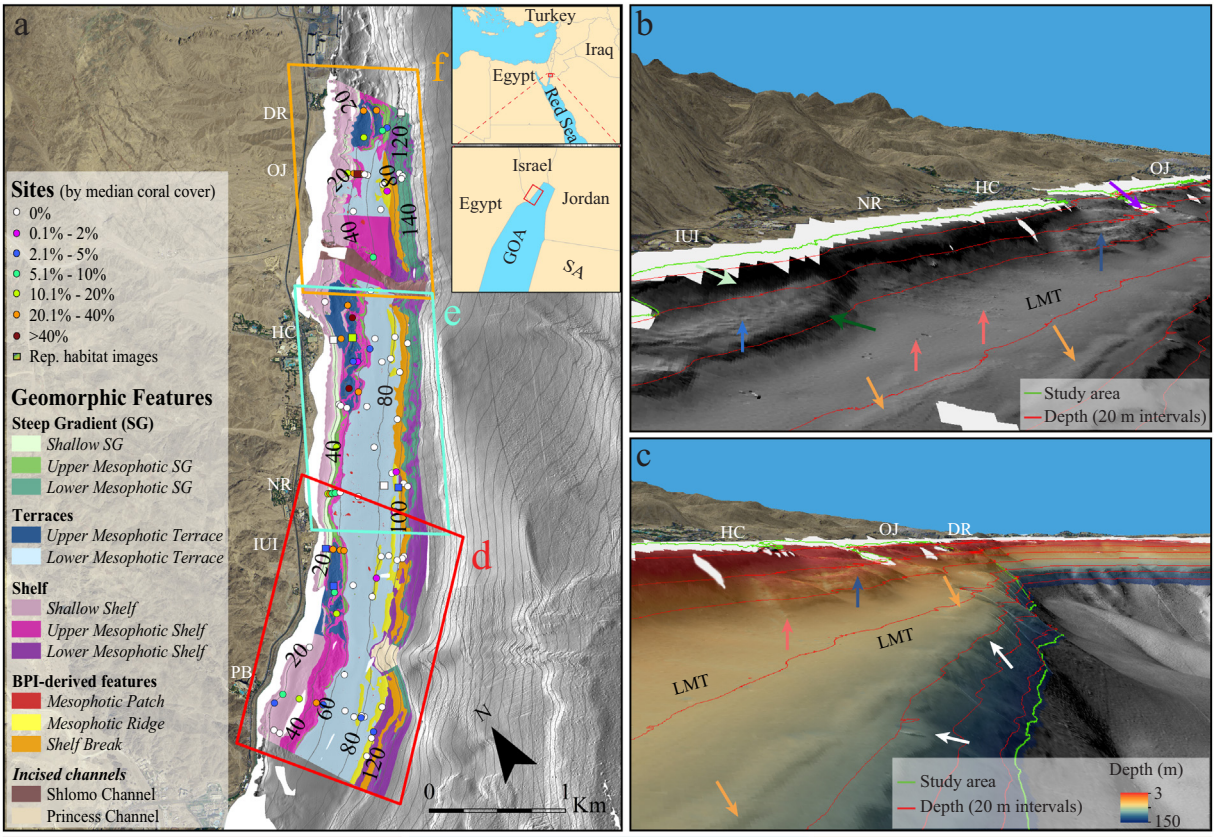
a
Sites (by median coral cover)
0%
0.1% - 2%
2.1% - 5%
5.1% - 10%
10.1% - 20%
20.1% - 40%
>40%
Rep. habitat images
Geomorphic Features
Steep Gradient (SG)
Shallow SG
Upper Mesophotic SG
Lower Mesophotic SG
Terraces
Upper Mesophotic Terrace
Lower Mesophotic Terrace
Shelf
Shallow Shelf
Upper Mesophotic Shelf
Lower Mesophotic Shelf
BPI-derived features
Mesophotic Patch
Mesophotic Ridge
Shelf Break
Incised channels
Shlomo Channel
Princess Channel
DR
OJ
HC
NR
IUI
PB
0
1
Km
N
Turkey
Iraq
Egypt
Red Sea
Israel
Egypt
Jordan
GOA
SA
b
OJ
HC
NR
IUI
LMT
Study area
Depth (20 m intervals)
c
HC
OJ
DR
LMT
LMT
Study area
Depth (20 m intervals)
Depth (m)
3
150

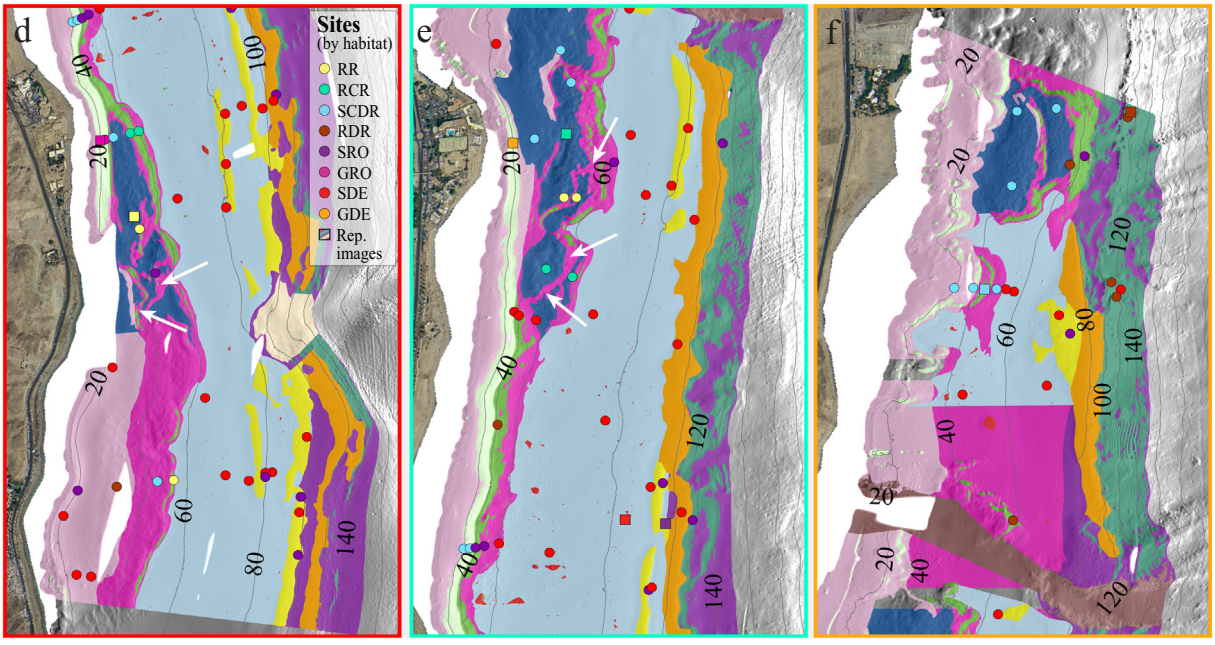
d
Sites (by habitat)
RR
RCR
SCDR
RDR
SRO
GRO
SDE
GDE
Rep. images
e
f

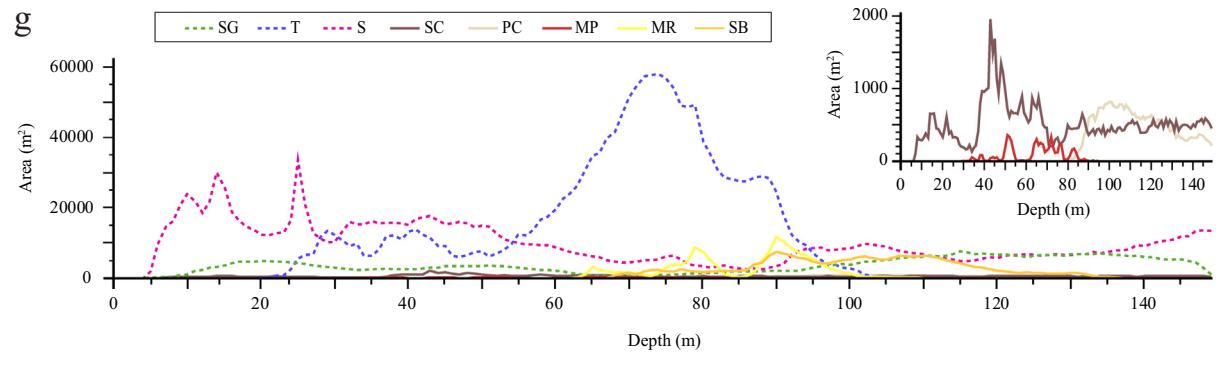
g
SG
T
S
SC
PC
MP
MR
SB
Area (m²)
Depth (m)
Area (m²)
Depth (m)

Fig. 1. Study area bathymetric and site data along the southernmost Israeli coastline of the Gulf of Aqaba. (a) Distribution of 12 newly defined geomorphology features (*italicized* names in map legend) and still imagery site locations (color-coded by benthic dataset-derived median hermatypic coral cover of all pictures per site) overlaying shaded-relief raster. Oblique three-dimensional shaded-relief projections scaled by bathymetry with 2× vertical exaggeration, angled to emphasize (b) southern upper mesophotic terrace (UMT) features, and (c) lower mesophotic terrace (LMT) features overlain by bathymetry. The study area outline (green) is vertically elevated for improved image quality. Projections include examples of upper mesophotic terrace features (blue arrows), shallow steep gradient (light green arrow) and upper mesophotic steep gradient (dark green arrow) features that help define the southern UMT, mesophotic ridge features (orange arrows), mesophotic patch features (pink arrows), shelf-break areas (white arrows), and a portion of the incised Shlomo Channel (purple arrow). White text in (a), (b), and (c), modified from Eyal et al. (2019), provide general locations used to assign site names (Supplementary Table 1) to geographical areas including Dolphin Reef (DR), Oil Jetty (OJ), Hotel Concentration (HC), Nature Reserve (NR), Interuniversity Institute (IUI), and Princess Beach (PB). (d) South, (e) middle, and (f) north maps provide a close-up of geomorphology features, with location and color-scheme provided in (a) and sites displayed by habitat type (Table 3). Habitat site legend for (e) and (f) found in (d) with abbreviations including rubbly reef (RR), rubbly coral reef (RCR), stony coral-dominated reef (SCDR), rock-dominated reef (RDR), sandy rock outcrop (SRO), gravelly rock outcrop (GRO), gravel-dominated expanse (GDE) and sand-dominated expanse (SDE) habitats. Colored squares identify locations of representative (rep) habitat images (Fig. 2). White arrows in (d) and (e) indicate the localized discontinuous nature of some UMT features. All maps are displayed with 20 m incremental bathymetric isobars beginning at 20 m depth and values are provided for study depth range in (a), (d), (e), and (f). White gaps on maps represent regions with no available bathymetric data (Tibor et al., 2010). (g) Zonal histogram of general (dotted lines) and geomorphology features defined without using any depth specification. Inset provides details for features with zonal distributions <2000 m^2. Abbreviation names in legend (g) include steep gradient (SG), terrace (T), shelf (S), Shlomo Channel (SC), Princess Channel (PC), mesophotic patch (MP), mesophotic ridge (MR), and shelf break (SB). Bathymetric position index (*BPI*), Saudi Arabia (*SA*).

cadaster, and geoinformatics; http://mapi.gov.il/). Incised channels relatively perpendicular to the shore, identified with bathymetry (Fig. 1c) and from previous studies (Makovsky et al., 2008; Tibor et al., 2010), were named according to region but were represented by a singular geomorphology feature category. The remaining study area was then classified as shallow, upper mesophotic, or lower mesophotic shelf geomorphology features (Table 1 definition modified from International Hydrographic Organization (IHO), 2013), with divisions following the same criteria applied for steep gradients.

Bathymetric position index (BPI) analysis, based on changes in slope position and elevation between reference and surrounding locations to classify seascape structures (Lundblad et al., 2006; Walbridge et al., 2018), has been found useful for identifying geomorphology features at mesophotic depths (Lundblad et al., 2006). Following initial geomorphology classification, discrete elevated structures smaller than the previously documented geomorphology features were identified atop terraces and shelves using bathymetry, slope, and hillshade rasters, and exaggerated 3D imagery generated in ArcScene (e.g. Fig. 1b). The structures were subsequently quantified with a BPI by applying the ArcGIS Benthic Terrain Modeler (BTM; Walbridge et al., 2018) to the original bathymetry and low-resolution addition. The structures and a notable BPI trend were classified as mesophotic patch (MP), mesophotic ridge (MR), and slope break (SB) geomorphology features.

Scale-factors of 50 and 400 were selected for fine-scale and broad-scale BPI analyzes, respectively (inner radius = 3 and 10, outer radius = 25 and 200, cell size = 2). These values reflected the approximate shortest and longest distances (Lundblad et al., 2006), measured relatively perpendicular to the shoreline, between initially identified elevated structures. BTM was used to create a standardized fine-scale BPI raster. Unitless BPI values herein are reported after standardization. After modifying to only include positive (elevated) BPI values less than steep gradients and using expanding and shrinking techniques to clean the data, the fine-scale raster was converted to polygons with some manually separated from adjacent features when applicable. BPI analysis was not employed for UMT features and below SB features because artifacts in the processed bathymetry prevented the identification of additional distinctive structures. After using ArcGIS to map the features based on new regional definitions (Table 1, modified from International Hydrographic Organization (IHO), 2013 for MP and SB), MR and MP polygons with surface areas >100 m^2 were deleted if no noticeable relief was identified in hillshade rasters. Trailing SB artifacts perpendicular to the shore were also manually eliminated if possible. The selection of surface area and BPI metric values were determined by bathymetry visual examination. Manual corrections were needed to resolve resolution artifacts related to initial multibeam processing. Still, the same method could be used for other reef systems when selecting different regional-specific values. Once identified and corrected, the area occupied by MP, MR, and SB features was removed from the underlying features they resided on. Elevated regions likely associated with incised channels were not classified as MP, MR, or SB features. ArcGIS was also used to estimate maximum average MP and MR feature topographic relief (methodology found in the Supplementary) and to generate select cross-sectional profiles to qualitatively evaluate relief.

All defined geomorphology features were converted to polygons and smoothed with a 20 m tolerance. Some polygon features were merged into larger adjacent polygons and outliers were removed after manually examining the bathymetry. ArcGIS polygon shape areas provided the plan surface cover of each feature. Zonal depth statistics for all features and hypsometric curves binned in 1 m increments for features not explicitly defined using depth were produced with ArcGIS zonal statistics and zonal histogram tools, respectively.

3.2. Still imagery acquisition

In total, 1726 images were acquired from 94 georeferenced sites using an opportunistic approach to maximize data retrieval from difficult to access depths. This approach resulted in an uneven number of pictures per site and sites per geomorphology feature. Final coordinates of the 94 sites were subsequently plotted as points in ArcGIS over bathymetry and geomorphology allocations (Fig. 1). The imagery was either newly acquired or obtained from previous studies.

Images from 67 sites were collected between February and December 2018 using a drop-camera system. The system consisted of a GOPRO Hero3 capturing plan-view images every 2–5 seconds, a custom-made camera tethered to the boat with a coax cable for live plan-view video, and a custom-made light source. Both cameras were mounted on a quadrapod positioned over a photo-quadrat frame (50 × 70 cm) with an attached dive computer to confirm depth. Drop depths were limited between 20 and 120 m to stay beyond shallow-water boat traffic restrictions and avoid camera operational limits. Sites were selected using a stratified random or even distribution sampling design (see Supplementary Table 1) to survey geomorphology features initially identified or to extend previous linear transect sampling profiles perpendicular to shore (Tamir et al., 2019). A handheld GPS (GARMIN, eTrex 10) receiver was used to fix the position of each site prior to image collection. A conservative 20 m horizontal coordinate error was estimated, varying with current speed and depth, with no error in depth as a result of dive computer verification. Some site coordinates were manually adjusted when considering prevailing currents and attached dive computer results, or when multiple GPS coordinates taken at a single drop were merged and represented by the center of all single-drop coordinates (Supplementary Table 1, bolded coordinates). Depending on sea conditions, 2–35 non-overlapping pictures were acquired as the boat moved above with prevailing currents at each site. This technique allowed for qualitative analysis of site areas from overhead imagery collected when dropping and raising the camera (Fig. 2).

Additional sites were established using multiple techniques. Reanalysis of available imagery (1–3 pictures per site) previously collected with a drop-camera system (Winters et al., 2017) provided five sites. Previously conducted 50 m photo transects parallel to shore along four linear profiles perpendicular to shore (Tamir et al., 2019) provided 19 sites. Three new sites were also acquired by conducting 50 m transects using the same method as Tamir et al. (2019) in May 2018 along a new opportunistic

Table 1
General definitions (provided without depth-specific divisions), number of study sites, area, and zonal statistics of 12 geomorphology features. Zonal statistics for incised channel feature is provided by individual channels (*italicized*). Bathymetric position index (BPI) values are reported after standardization. Standard deviation (*STD*), no still imagery available for the feature (*NA*).

Geomorphology features (abbreviation)		# of sites	Area (km^2)	% Study area	Mean depth (m)	Depth STD	Depth (m) min-max [range]	Feature definitions
Shallow Steep Gradient (SSG)		5	0.09	2.5	22	7	3-36 [33]	
Upper Mesophotic Steep Gradient (UMSG)		11	0.09	2.3	51	9	32-76 [44]	Areas with slopes primarily ≥20°
Lower Mesophotic Steep Gradient (LMSG)		8	0.28	7.6	124	16	75-150 [75]	
Upper Mesophotic Terrace (UMT)		16	0.23	6.2	38	8	20-61 [41]	Linear, primarily flat (slopes ≤10°) areas with extensions deeper than 20 m partially bound to some extent (see white arrows in Supplementary Fig. 1b) by nearby (~0-90 m) landward ascending steep gradients and seaward descending steep gradients
Lower Mesophotic Terrace (LMT)		22	1.23	33.1	73	11	24-104 [80]	
Shallow Shelf (SS)		9	0.50	13.4	20	8	5-36 [31]	Primarily gently sloping (<20°), non-channel regions between the shore and deepest mapped areas not bounded by steep gradients
Upper Mesophotic Shelf (UMS)		4	0.43	11.7	50	10	34-76 [42]	
Lower Mesophotic Shelf (LMS)		NA	0.38	10.4	123	22	74-150 [76]	
Mesophotic Patch (MP)		2	0.01	0.2	65	13	31-94 [63]	Individual or assemblages of elevated structures (e.g. pink arrows in Fig. 1b) with surface areas <1500 m^2 atop LMT and UMS features
Mesophotic Ridge (MR)		14	0.14	3.7	86	9	63-110 [47]	Linear, moderately elevated (BPI maximum values <100) structures with surface areas >1500 m completely or partially overlaying LMT features
Shelf Break (SB)		3	0.23	6.1	101	14	68-137 [69]	Discrete linear regions overlaying a marked increase in slope at the seaward margin if part of the feature was distinct (BPI maximum values >250) from the surrounding area
Incised Channel	*Princess Channel (PC)*	NA	0.03	0.9	114	17	82-150 [68]	Channels identified from bathymetry and previous studies, excluding isolated small flatter (<20°) areas encircled or bordered by steeper (≥20°) areas in shallowest and deepest parts of Shlomo Channel
	Shlomo Channel (SC)	NA	0.08	2.0	77	40	7-150 [143]	
Study area			3.70[a]		71	36	3-150 [147]	

[a]Value different than sum of areas because of polygon smoothing

perpendicular linear profile near the hotel concentration (HC) geographical area (Fig. 1a). The middle of each 50 m transect was set to represent one georeferenced site along each of the five linear paths used for the current study. Apart from a 60 m transect site (NR6, Supplementary Table 1) visually classified as 100% sand cover, 19–72 non-overlapping images were acquired at each 50 m transect site.

3.3. Benthic and lithologic cover analysis

Photographs were imported into 'CoralNet' (http://coralnet.ucsd.edu/) to determine benthic and lithologic cover by categorizing the entities below each of 100 randomized points placed within the photo-quadrat per picture (Beijbom et al., 2012). Two related but separate datasets were generated by first examining the benthic cover and then the lithologic cover within each image. For this study, benthic cover represented major sessile reef organisms or substrate if no biota was visible. Lithologic cover represented all hard material, including material found under non-calcifying organisms, such as clastic sediment, calcifying organisms' skeletons, and other carbonate deposits that presumably could preserve in the geologic record. The benthic dataset was divided into 11 categories (eight biological and three substrates) and the lithologic dataset was divided into six categories (Table 2). The hermatypic coral category (which included the hydrocoral *Millepora* spp.) was subdivided by coral genus (benthic dataset) and coral growth form (lithologic dataset) based on existing regional genera morphology nomenclature (see Tamir et al., 2019 and Coraltraits.org). Still, growth forms of some GoA species can change with depth (Eyal et al., 2019; Tamir et al., 2019). Unless otherwise mentioned, benthic and lithologic percent cover for each category (Table 2) was summarized by the median of the number of pictures that were used for a particular analysis per site to better represent variable, skewed datasets. Lithologic and benthic category medians were calculated for all geomorphology features where still imagery was available (all but incised channel and lower mesophotic shelf features). For additional statistical analyses, data were imported as abundance counts, square-root transformed, and used to produce Bray-Curtis similarity resemblance matrices with R software (R Core Team, 2020).

3.4. Habitat classification

Site median lithologic dataset results from all pictures were used for K-means clustering to examine potential habitat classifications for the 94 sites. The optimal number of clusters was determined with the {NbClust} package using the Calinski–Harabasz index in R. The cluster number was validated using the average silhouette coefficient (Si). Clusters returned were further tested statistically using multiple response permutation procedure with 999 permutations in the R {vegan} package (Oksanen et al., 2018). Habitat group classifications were based on original clusters after a visual examination of plan overhead images (e.g. Fig. 2b-d). A one-way Similarity percentage analysis (SIMPER) was subsequently performed using PRIMER v7 (PrimerE Ltd., Ivybridge, UK) to determine within-group similarity and identify which lithologic categories contributed most to dissimilarities (Clarke and Gorley, 2015).

3.5. Comparisons with geomorphology

To avoid potentially biased results due to the high variation in sample sizes, new datasets (unbalanced design) were created by randomly subsampling 5–20 pictures per sites found on geomorphology features

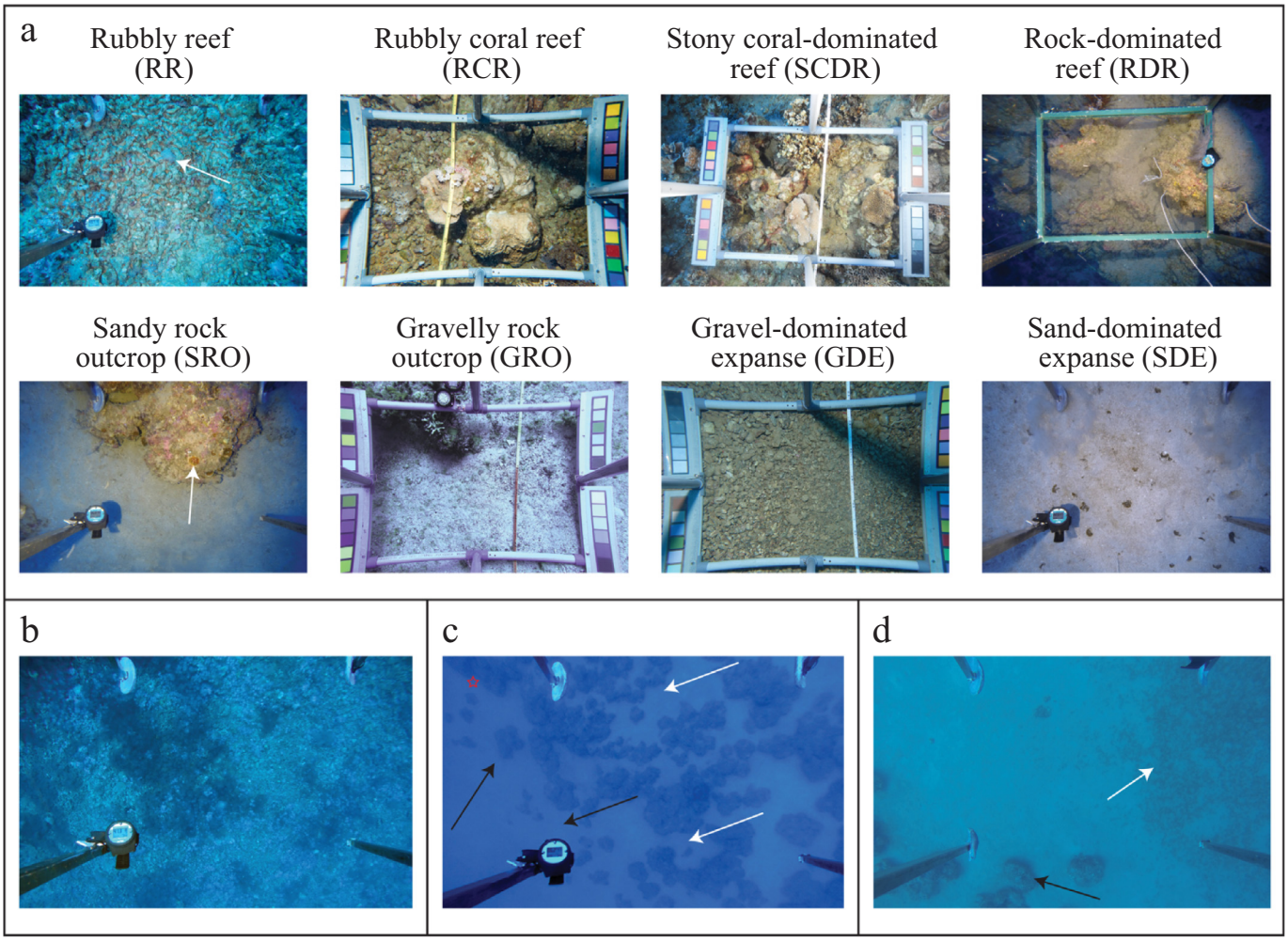

Fig. 2. Still imagery and examples of habitat classification. (a) Representative images of each habitat classification group. Image locations are indicated by squares in Fig. 1 and site names are provided in Supplementary Table 1. White arrows for RR and SRO identify a living *Alveopora* sp. colony, the primary coral rubble producer on GoA upper mesophotic terraces, and a living *Leptoseris* sp. colony, the most frequent coral found at lower mesophotic habitats in the region, respectively. (b) Overhead drop-camera view of RR representative image, showing an extensive rubble field with low relief. (c) Overhead drop-camera view of SRO representative image (red star provides exact location), with visually higher relief than (b). Black arrows indicate the border between SRO and a neighboring SDE habitat, demonstrating how the transition between habitat types may be gradational (the border has less rocky cover than further within the habitat at the upper right of the picture). The image also shows how sandy channels and patches (white arrows) are often found cutting through main habitat features. (d) Overhead drop-camera view of mesophotic patch geomorphology feature (site number OJ4), demonstrating how this feature type may consist of aggregated hard substrate (black arrow) often surrounded by sandy areas or seagrass (white arrow). This site was quantified as 100% sand cover and clustered with SDE sites based on two random drops within sand. The dimensions of all quadrats in pictures are 50 × 70 cm.

with at least four sites. Sites with <5 pictures were not included except site NR6, where results were included based on a qualitative assessment that constituted an area spanning >4 pictures. Unbalanced design datasets (selected pictures identified in Supplementary Table 2) included eight of the newly defined geomorphology features. Balanced design datasets (four sites per geomorphology feature) were created with random subsampling from the unbalanced design datasets (selected sites identified in Supplementary Table 1). The subsampling procedure substantially reduced variability and improved overall analysis accuracy. Non-metric multidimensional scaling (NMDS) plots were generated from the balanced design datasets, based on Bray–Curtis distance matrices using the {vegan} package in R package, to visually depict variations among geomorphology features. PERMANOVA analyses were performed to test for the significance of the observed groups and were followed by pairwise comparisons (999 permutations).

3.6. Comparisons with seafloor complexity and environmental variables

Seafloor complexity and environmental rasters were calculated to examine potential relationships with mesophotic reef benthic and lithologic cover and spatial distributions (Costa et al., 2015; Linklater et al., 2016; Suka and Rooney, 2017). All seafloor complexity rasters and associated site-specific values were calculated from the original bathymetry dataset using the same cell size and resolution; BTM was used to generate all seafloor complexity rasters (Walbridge et al., 2018). Surface area to planar area (SAPA) calculations were run with the corrective option and terrain ruggedness calculations were conducted at size three (Walbridge et al., 2018). Distance from shore was calculated with the ArcGIS Euclidean Distance tool. Regional light attenuation coefficients (K_dPAR, calculated for the top 30 m water column depths) were measured to provide annual (2014–2015) and summer (July–August 2015) averages interpolated with an ~1–2 km distance (resolution) between 19 measurement points (Tamir et al., 2019). K_dPAR values of the closest available data points were used for study sites (11 in total) shallower than 30 m when necessary after interpolation (Supplementary Table 3). The Massachusetts Institute of Technology general circulation model (MITgcm; Marshall et al., 1997) provided approximate regional near-bottom (deepest grid-cell values for the given location) temperature and water current rasters and a sea surface temperature raster for the year 2012 with a horizontal resolution of 300 × 300 m (details in Supplementary). Based on the horizontal resolution, we applied 2-dimensional linear interpolation for MITgcm output to obtain the

Table 2
Definition or examples of benthic and lithologic cover categories. *Italicized* benthic categories indicate live biological cover.

Dataset	Category	Description or example
Benthic	*Hermatypic coral*	Live scleractinian coral and *Millepora* spp. (full list in Supplementary Table 4)
	Antipatharia	Referred to as black corals
	Soft coral	Other coral without calcareous skeletons including *Discosoma*, Hydrozoans, and Alcyonacea
	Other sessile invertebrates	Including Ascidians, Actiniaria, and Bivalves
	Sponges	All macroscopic Porifera observed
	Algae	Macroalgae and turf algae
	Crustose coralline algae (CCA)	Identified as CCA, regardless of underlying substrate
	Seagrass	*Halophila stipulacea* (most common species; Winters et al., 2017)
	Hard substrate	Dead coral, beach rock, or predominately carbonate bedrock probably immoveable by hand
	Gravel	Unattached sediment with an approximate diameter >2 mm
	Sand	Unattached sediment and shell fragments with an approximate grain diameter ≤2 mm
Lithologic	Hermatypic coral	Live scleractinian coral and *Millepora* spp. (full list in Supplementary Table 4)
	Crustose coralline algae (CCA)	Only classified if attached to hard substrate
	Coral rubble	Dead, unattached rock apparently derived from coral with approximate grain diameter >2 mm
	Hard substrate	Dead coral, beach rock, or predominately carbonate bedrock probably immoveable by hand
	Gravel	Unattached sediment with an approximate diameter >2 mm, not including coral rubble
	Sand	Unattached sediment and shell fragments with an approximate grain diameter ≤2 mm

values underneath the measured sites representing the most likely estimates of position and environmental factors. Given the employment of this method, as well as our use of a 20 m polygon smoothing tolerance and assumption of a 20 m horizontal site error, our site values represent the best available estimates of seafloor complexity and environmental variables without necessitating rescaling raster resolution.

A Draftsman plot was generated to identify which variables required transformation and showed co-linearity. Nine potential influencing seafloor complexity and environmental parameters were selected (depth, slope, aspect, curvature, terrain ruggedness, K_dPAR summer at 30 m, K_dPAR yearly at 30 m, horizontal current near-bottom velocity, and SAPA) after normalization. Only values for terrain ruggedness were log-transformed. The selected subset of variables was tested for significance using 999 permutations. The BIOENV procedure has been used to explore and identify seafloor complexity and environmental variables that best correlated with the benthic community structure at mesophotic depths (Linklater et al., 2016). Using BIOENV from the BEST tool in PRIMER v7, the top subset of tested influential parameters was selected by the set of seafloor complexity and environmental variables showing the highest correlation which best described the overall community pattern (Clarke and Ainsworth, 1993). To optimize the procedure and to avoid redundancy, BIOENV analysis was first performed without a permutation test to identify and exclude low contributing variables. Then, the procedure was performed with 999 permutations for the remaining variables in the datasets, with site and geomorphology as fixed factors. To further determine specific factors that correlated with benthic composition, a nonparametric multivariate regression was applied between normalized environmental and seafloor complexity variables and balanced design site composition (benthic and lithologic) datasets based on Bray–Curtis similarity matrices implemented as distance-based linear models (DistLM; 999 permutations). Specifically, the DistLM routine, used to quantify the relative contribution of each environmental/geomorphology variable to the variability in benthic and lithologic composition, was performed with a step-wise selection procedure based on the Akaike Selection Criterion (AICc) using PRIMER7 and PERMANOVA+.

4. Results

4.1. Regional geomorphology

Overall, 12 geomorphology features with distinct definitions were identified within the GoA spanning the mesophotic zone (Fig. 1a). The lower mesophotic terrace (LMT) features occupied the largest portion (33.1%) of the study area; the discontinuous (white arrows in Fig. 1d, e) upper mesophotic terrace (UMT) features had a smaller depth range than LMT features (Table 1). Steep gradient features covered a small area (<15%) primarily concentrated at depths ≥75 m (Table 1). The 12 documented mesophotic ridge (MR) features were narrow (widths <100 m), and generally linear and parallel to the shoreline (Fig. 1) with an average approximate maximum relief of 7.2 m ± 1.4 standard error (SE) above neighboring features. MR zonal area distribution depth centered at 80 and 90 m (Fig. 1g). Mesophotic patch (MP) feature areas were generally circular to oval and small (median = 4 m^2). With a 0.7 m ± 0.8 SE approximate average maximum relief above neighboring features, MPs lack the steep-sided, high relief, and larger average diameter (25–35 m) characteristics of Australian Great Barrier Reef pinnacles (Abbey et al., 2011) common at mesophotic depths. Together, the 241 individual MP features detected constituted 0.2% of the study area with a shallower minimum and maximum depth but larger range than MR features (Table 1) and absent zonal depth peaks at 40 m, 55–60 m, and 78 m (Fig. 1g). Despite indiscernible detection of rugosity differentiation (Supplementary Fig. 1i, j), qualitative examination of shaded-relief (Fig. 1), bathymetry profiles, and estimated relief calculations implied LMT features had little topographic relief compared to adjacent BPI-derived (MP, MR) and UMT features (Fig. 1). Examination of imagery indicated boundaries between geomorphology features were not always discrete but often existed along transitions in benthic and lithologic cover (e.g. black arrow in Fig. 2c).

4.2. Benthic and lithologic cover and habitats

Overhead images highlighted relatively heterogeneous surface cover in the study area (Fig. 2b-d). However, the examination of all images per site led to the identification of distinct trends reported as the average of all 94 site medians ± the SE for each category henceforth in this section unless otherwise stated. Given site selection criteria (section 3.2 and Supplementary Table 1) and considering LMT spatial dominance, average cover constituted less sand than if a completely randomized sampling method was used. Still, from a lithologic perspective, sand was the most common substrate type sampled with an average median cover between all sites of 62 ± 4% (Supplementary Table 2). Site median hermatypic coral and coral rubble cover averaged 7 ± 1% and 8 ± 2%, respectively. Median hermatypic coral cover was highest at sites 30–60 m in depth whereas median coral rubble cover was highest at sites

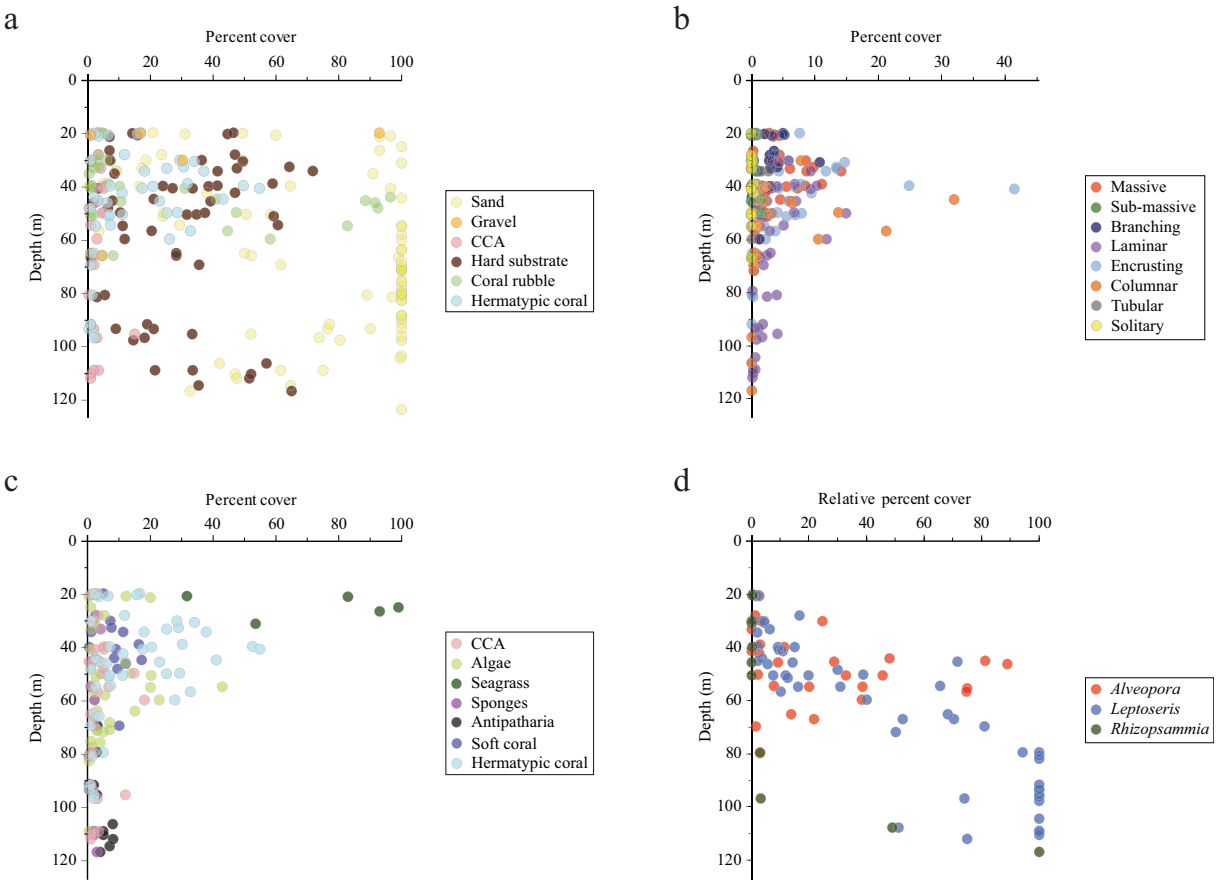

Fig. 3. Site composition versus depth. Lithologic percent cover of (a) all categories (Table 2) and (b) coral growth forms. Benthic percent cover of (c) all biological categories (Table 2) and (d) relative percent of hermatypic coral cover by the two most common genera in the study area (*Leptoseris* and *Alveopora*) and the only three genera identified at study sites with point-count analysis deeper than 75 m. Compositions are presented as the median of all picture point count results per site for (a) and (c), and as the mean of all picture point count results per site for (b) and (d). Graphs only display values where the category was present or non-zero at a particular site when considering point-count analysis. Crustose coralline algae (*CCA*).

40–60 m in depth (only depths where some sites had >20% and >30% average cover, respectively; Fig. 3a). However, even when using multiple images per site, study methodology may have resulted in lower coral cover because reefs in the region often included sandy channels that may average out denser coral cover areas (Fig. 2c, d). When examining the means of all images per site to include outliers and only considering sites with hermatypic coral (67% of sites, averaging 12 ± 2% hermatypic cover), the laminar growth-form dominated (41 ± 5%) and was the only growth-form besides columnar and encrusting found deeper than 75 m (Fig. 3b).

Benthic point-count analyses identified 49 coral genera with the potential to contribute carbonate to future reef development (Supplementary Table 4). Soft coral median cover had the greatest site maximums (>10% cover) at depths of 30–70 m while algae and seagrass median cover was greatest in shallower areas (>5% median cover never found deeper than 75 m and 35 m for algae and seagrass, respectively). Median Antipatharia cover was only found deeper than 60 m and was low but generally increased with depth to a high of 8% at 112 m (Fig. 3c). When examining the mean of all images per site to include outliers and only considering sites with coral present, *Leptoseris,* found at 55% of all sites (83% of sites with coral), was the most common genera on average (38 ± 5% of all coral per site). *Leptoseris* relative abundances primarily increased with depth and *Leptoseris* was the most common coral genera deeper than 70 m (Fig. 3d), often as small entrusting and plating colonies (Fig. 2, SRO; also see Kramer et al., 2020). *Alveopora*, found at 34% of all sites (51% of sites with coral), was the second most common genera on average (11 ± 3% of all coral per site), especially at depths between 30 and 70 m (Fig. 3d). *Rhizopsammia* (azooxanthellae coral) was the deepest (116 m depth) hermatypic coral genera identified with point-count analysis in the region and along with *Leptoseris* and *Alveopora* (zooxanthellae corals), was the only identifiable coral genera found deeper than 75 m (Fig. 3d).

Cluster analysis identified ten statistically significant groups ($p < 0.001$) in terms of lithology (Supplementary Table 1). Eight distinct habitats were described for the study area (Table 3) after manually consolidating the stony coral-dominated reef (SCDR) and the sandy rock outcrop (SRO) habitats (each originally consisted of two groups). Two sites (Supplementary Table 1, bolded habitat name) were regrouped as SCDR habitats because they better fit the habitat description (Table 3), as confirmed by manual examination of site images. SIMPER analysis indicated within-group habitat similarity >80% (Table 3). Sites with >15% median hermatypic coral cover were found only to identify as SCDR and rubbly coral reef (RCR) habitats but the hermatypic coral category was not the greatest contributor to within-group similarity. Sand was a major within-group similarity contributor for half of the habitats; the coral rubble category was the greatest contributor for both rubble habitats (Table 3). Sites classified as rubble habitats had a narrow depth range (41–60 m) and were only found on upper terraces and upper mesophotic steep gradients; sites classified within the SCDR habitat were never identified below 50 m but were still found on 50% of the geomorphology features where sites were studied. Gravel habitats were only found on shallow steep gradient features.

4.3. Comparisons with geomorphology, seafloor complexity, and environmental variables

Balanced design still imagery composition and NMDS plots grouped by geomorphology features (Fig. 4) show different benthic and lithologic

Table 3
Habitat categorization and SIMPER analysis. The number of associated study sites and depth information, associated geomorphology (geomorph) features, SIMPER analysis, and descriptions are provided for each habitat type. *Italicized* text indicates when only one site with the habitat classification is found within a particular geomorphology feature. Habitat categories classified as including biogenic and/or rocky reefs are underlined. SIMPER analyses are based on the lithologic dataset including all pictures. These analyses provide the average similarity (Sim%), major lithologic category contributors (cumulative similarity >70%) with the first category contributing the most, and associated lithologic category cumulative contributions (Cum%). Abbreviations for geomorphology features include: shallow steep gradient (SSG), upper mesophotic steep gradient (UMSG), lower mesophotic steep gradient (LMSG), upper mesophotic terrace (UMT), lower mesophotic terrace (LMT), shallow shelf (SS), upper mesophotic shelf (UMS), mesophotic patch (MP), mesophotic ridge (MR), and shelf break (SB). Standard error (*SE*).

Habitat (abbreviation)	# of sites	Depth (m) min-max [range]	Average depth (m) (± SE)	Associated geomorph.	SIMPER analysis			Habitat description
					Sim%	Contributors	Cum%	
Rubbly reef (RR)	5	44–55 [11]	48 ± 2	*UMSG*, UMT	88.90	Coral rubble	78.83	Reefs dominated (≥ 70%) by coral rubble cover but very low (< 10%) live hard coral cover
Rubbly coral reef (RCR)	5	41–60 [19]	50 ± 4	UMSG, UMT	85.48	Coral rubble Hermatypic coral	39.88 71.16	Reefs with high or greater (≥ 30%) coral rubble cover and moderate or greater (≥ 15%) live hard coral cover
Stony coral-dominated reef (SCDR)	14[a]	20–50 [30]	35 ± 2	SS, SSG, *UMSG*, UMS, UMT	81.76	Hard substrate Hermatypic coral	43.75 76.63	Coral reefs with moderate or greater (≥ 15%) live hard coral cover, very high (≥ 50%) attached substrate[b] cover and low (< 15%) coral rubble cover
Rock-dominated reef (RDR)	8	28–117 [89]	78 ± 13	LMSG, *SS*, UMSG, *UMT*	85.01	Hard substrate Sand	53.45 94.18	Regions of sand and rocky reefs (≥ 40% hard substrate cover and low (< 15%) live hard coral cover)
Sandy rock outcrop (SRO)	16	21–115 [94]	78 ± 7	LMSG, MR, *SS*, UMS, UMSG	84.49	Sand Hard substrate	56.30 90.10	Regions with very high (≥ 50%) sand cover and very low to very high (10–50%) hard substrate cover
Gravelly rock outcrop (GRO)	2	20–30 [10]	25 ± 5	SSG	90.62	Sand Gravel Hard substrate	42.48 67.27 83.50	Regions with moderate to dominant (15–70%) gravel cover and some cover (≥ 5%) of attached substrate[b] outcrops
Gravel-dominated expanse (GDE)	1	–	20[c]	*SSG*	–	–	–	Gravel-dominated expanse (≥ 85% gravel cover)
Sand-dominated expanse (SDE)	43	21–124 [103]	70 ± 4	*LMSG*, LMT, MP, MR, SB, SS, UMSG, *UMT*	95.35	Sand	99.50	Sandy expanse (≥ 85% sand cover), possibly surrounding isolated, very low cover (< 10%) hard substrate outcrops and/or overlain with seagrass

[a]Two sites (OJ1 and NR1) originally clustered with RDR but were moved to SCDR because they better matched the habitat description, especially when observed from overhead images
[b]Includes hermatypic coral, hard substrate, and CCA categories
[c]Represents one depth, as only one site matched the criteria for this habitat

cover distributions, particularly between the lower mesophotic terrace (LMT), upper mesophotic terrace (UMT), and lower mesophotic steep gradient (LMSG) features. Hermatypic coral was found at all geomorphology features where images were obtained (Supplementary Table 2) but was rare (<3%) at mesophotic ridge (MR), mesophotic patch (MP), and shelf break (SB) features and not present within the balanced design dataset for LMSG and LMT features (Fig. 4a, b). Site median average balanced design coral cover was highest on UMT features (Fig. 4a,b), which also harbored the peak quadrat coral cover (97%, site HC3 in lithologic dataset). Results imply coral carbonate production is currently highest on UMT features, especially in the northern UMT, which hosts stony coral-dominated reef (SCDR) habitats (Fig. 1f), moderate rugosity (Supplementary Fig. 1i, j), and towering carbonate structures seen in drop camera images. Shallow and upper mesophotic steep gradient (SSG and UMSG, respectively) and upper mesophotic shelf (UMS) features also had a balanced design site median average live coral cover >10%. With the highest average sand cover (Fig. 4a, b), unbalanced design study sites on LMT features were most closely associated with sand, followed by MR and LMSG features (Supplementary Fig. 2a). Notable coral rubble site median average cover (>20%) was restricted to (Fig. 4a), and most associated with (unbalanced design; Supplementary Fig. 2b), UMSG and UMT geomorphology features; hard substrate areas were abundant, with lithologic balanced design site median averages >20% at all but LMT features. Peak lithologic categorial cover by quadrat was found on UMT and UMSG features for coral rubble (100%, sites PB7 and IUI5, respectively), and on a LMSG feature for hard substrate (100%, site OJ13).

From a biological perspective, UMT features were most associated with hermatypic and soft corals (unbalanced design; Supplementary Fig. 3a, b), and exhibited the greatest balanced design site median average cover per geomorphology type (Fig. 4b). The coral genera *Alveopora* was most commonly found associated with UMT and UMSG features; *Leptoseris* was most commonly associated with UMSG, as well as MR and UMS features (unbalanced design; Supplementary Fig. 3c, d). Antipatharia and crustose coralline algae (CCA) were found on all geomorphology feautres that images were obtained from except on MP (only represented by two sites) and LMT features for Antipatharia and CCA, respectively. However, Antipatharia and CCA balanced design site median average cover were low (<5%) and only recorded at MR and LMSG sites (for Antipatharia; Fig. 4b). Algae was found on all features except SBs but balanced design site median average cover only exceeded 5% on UMSG and shallow and upper mesophotic shelf features (SS and UMS, respectively). Peak benthic categorial covers by quadrat were found on UMSG features for CCA and algae categories (52%, site IUI9 and 81%, site PB7, respectively), on SS features and shallow steep gradient (SSG) features for seagrass (100%, sites PB1, PB3, and IUI2, and 100%, site HC1, respectively), on an UMS feature for Antipatharia (63%, site NR5), and on an UMT feature for soft coral (100%, site IUI5).

Significant differences in overall community lithologic and benthic composition between specific geomorphology features were detected; >50% of differences (R^2) were attributed to cover composition for both study designs (Table 4). Pairwise analysis of balanced design datasets (Table 4) indicated 68% (benthic) and 54% (lithologic) of all possible combinations had differences with *p*-values <0.05. Notably, LMT features were significantly different than all analyzed features (except LMSG features), including adjacent mesophotic ridges, which were also significantly different from all other features except LMSG features as well as SS features (lithologic perspective).

When considering balanced design benthic and lithologic assemblage structure, BIOENV procedure indicated results with p-values <0.05 with lower than 50% correlations at both site and geomorphology levels (Table 5). Depth and aspect (direction) were identified as the best combination of variables to explain multivariate distributions at the site level but depth and slope, and summer K_dPAR best explained site

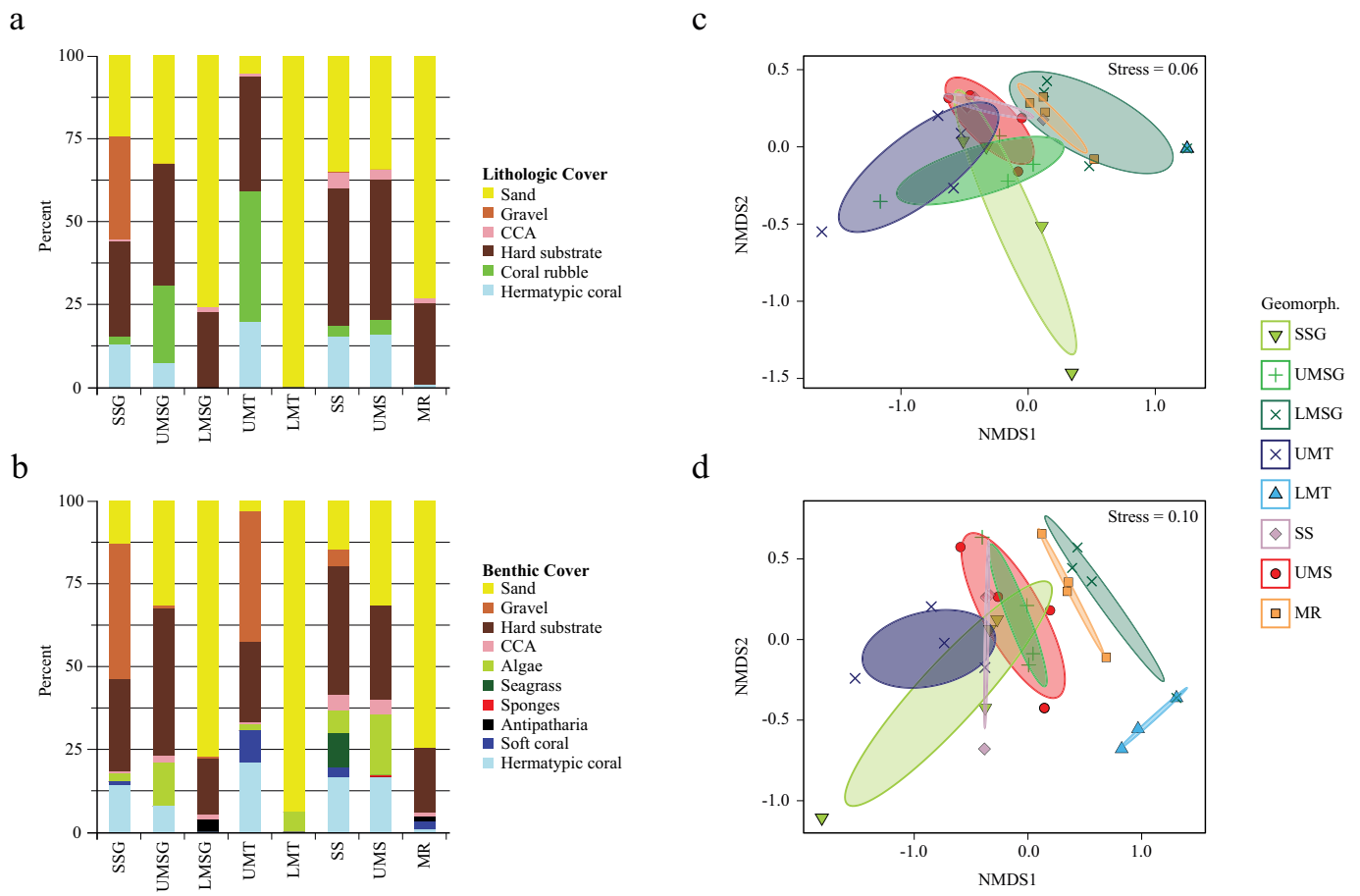

Fig. 4. Balanced design lithologic and benthic still imagery composition plotted by geomorphology features. (a) and (b) display average site median lithologic and benthic composition, respectively. Non-metric multidimensional scaling (NMDS) plots of (c) lithologic and (d) benthic data derived from cover percentages at geomorphology features ($n = 4$ sites per geomorphology). Standard error ellipses show 95% confidence areas of geomorphology features, and each symbol represents the community composition found at a particular site, based on Bray-Curtis dissimilarity. Multiple sites on the lower mesophotic terrace (LMT) feature overlap. Abbreviations for geomorphology (geomorph) include: shallow steep gradient (SSG), upper mesophotic steep gradient (UMSG), lower mesophotic steep gradient (LMSG), upper mesophotic terrace (UMT), lower mesophotic terrace (LMT), shallow shelf (SS), upper mesophotic shelf (UMS), mesophotic ridge (MR). Crustose coralline algae (*CCA*).

distributions by geomorphology for the benthic and lithologic datasets, respectively. DistLM revealed that depth and annual K_dPAR explained 40% of the variation in the benthic communities while depth only accounted for 25% of the lithologic community compositions (Table 5).

5. Discussion

5.1. Geomorphology map and mesophotic reef identification

Study results provide a new georeferenced geomorphology map with formally defined structural features useful for interpreting past reef development and identifying modern mesophotic reefs in the GoA. Despite sandy lower mesophotic terrace (LMT) features spanning nearly a third of the study area (Table 1), upper mesophotic terrace (UMT) and lower mesophotic steep gradient (LMSG) features hosted some sort of biogenic and/or rocky reef habitat (underlined in Table 3) except for one site per feature. This implies at least 13.8% of the study area may consist of mesophotic reefs, although higher coverage is likely considering mesophotic reef habitats were also found atop other geomorphology feature types (Fig. 1). While some features (UMT and LMSG) provide a reasonable geospatial prediction for mesophotic reef development, only half of the mesophotic ridge (MR) sites were classified as rocky reef habitats (sandy rock outcrop). Therefore, these features cannot reliably predict the presence of mesophotic reefs. Still, identification of habitat and geomorphology features overall improves our ability to map MCEs in the region. Additionally, the examination of still imagery and geomorphology provides new insight into GoA modern lithologic and benthic mesophotic reef patterns and geomorphology formation at modern mesophotic depths.

5.2. Modern mesophotic benthic/lithologic cover and geomorphology

Beyond classifying and mapping new geomorphology features in the GoA, study results identified significant differences (Table 4 and Fig. 4c, d) as well as recognizable associations between underlying geomorphology features and benthic and lithologic cover. Much of the study area between 60 and 100 m was a barren sandy expanse. This is similar to results from Bridge et al. (2011), who suggested a lack of topographic highs along flat terraces on Australian mesophotic reef shelf margins could facilitate the development of extensive sandy regions. However, GoA topographic high MR and mesophotic patch (MP) features adjacent to the sandy expanse provided elevated substrates towering over MR and MP sand cover that supported the proliferation of unique reefal/rocky outcrop habitats (Table 3) with an average biological cover (italicized categories in Table 2) >35% when considering all pictures and not including the sand category in calculations.

Another major association between geomorphology and surface cover was identified from the habitats composed of unconsolidated coral rubble (RCR and RR; Fig. 2) and primarily unattached live corals. Study sites categorized as these habitats were only found on upper mesophotic terrace (UMT) features and on upper mesophotic steep gradient (UMSG) features below terraces (Table 3; except site PB7).

Table 4
One-way PERMANOVA (left) and pairwise comparisons (right) for benthic and lithologic median datasets by geomorphology feature when 5–20 pictures were subsampled per site. One-way PERMANOVA results provided for both the unbalanced and the balanced study designs. Pairwise comparisons, only provided for the balanced study design, are reported as *p*-values, with values <0.05 in bold. Abbreviations for geomorphology features include: shallow steep gradient (SSG), shallow shelf (SS), upper mesophotic steep gradient (UMSG), upper mesophotic shelf (UMS), upper mesophotic terrace (UMT), lower mesophotic steep gradient (LMSG), lower mesophotic terrace (LMT), and mesophotic ridge (MR). Degrees of freedom (*Df*), not available (*NA*, the test statistic was negative).

Dataset (study design)	Df	Pseudo-F	R^2	p-value
Benthic (unbalanced)	7	11.211	0.606	**0.001**
Benthic (balanced)	7	5.757	0.627	**0.001**
Lithologic (unbalanced)	7	9.520	0.566	**0.001**
Lithologic (balanced)	7	4.970	0.592	**0.001**

Lithologic dataset \ Benthic dataset	SSG	SS	UMSG	UMS	UMT	LMSG	LMT	MR
SSG	-	0.414	0.245	**0.044**	0.637	**0.029**	**0.030**	**0.027**
SS	0.265	-	0.516	0.275	0.148	**0.030**	**0.023**	**0.028**
UMSG	0.452	0.939	-	0.920	**0.033**	**0.030**	**0.022**	**0.029**
UMS	0.261	NA	0.734	-	**0.023**	**0.023**	**0.026**	**0.029**
UMT	0.060	**0.028**	0.378	0.093	-	**0.024**	**0.026**	**0.026**
LMSG	**0.025**	0.077	**0.042**	**0.029**	**0.031**	-	0.084	0.473
LMT	**0.036**	**0.025**	**0.027**	**0.031**	**0.024**	0.133	-	**0.034**
MR	**0.035**	0.096	**0.024**	**0.027**	**0.017**	0.526	**0.031**	-

Despite lower topographic relief than coral framework-dominated habitats, GoA rubble-dominated habitats still harbored dynamic mesophotic reef communities with coral cover often greater than at shallower depths (Eyal-Shaham et al., 2016). A qualitative examination found that regional coral genera classified with columnar growth-forms (*Alveopora, Euphyllia, Rhizopsammia*) were the main preserved coral rubble constituents on upper mesophotic reefs and generated unconsolidated vertical accumulations. We speculate rubble in these habitats was primarily produced on flat UMT areas and also produced and/or transported to adjacent deeper steep gradients (Eyal et al., 2019). Conditions needed for these genera to dominate and produce coral rubble field habitats (RCR and RR) were found associated with some (44%), but not all sites located on UMT features (Fig. 1). The association was greater (58%) when removing the northernmost UMT features that were never considered rubble habitats (Fig. 1f), implying GoA mesophotic coral rubble reef habitats are associated with UMTs and additional unknown factors. Rubbly habitats generally had higher average sea surface temperatures than sites categorized by other habitats found on UMT and UMSG features (Supplementary Fig. 1 and Supplementary Table 3). However, the differences were small, and a limited number of sites prevented further statistical comparisons. These and other potential differences in environmental and complexity parameters were unclear and warrant finer-scale examination to determine what properties or associated environmental conditions promote the accumulation of large, low-relief live coral and coral rubble fields.

Overall, depth was identified as the largest significant contributing variable explaining observed differences among site community compositions and geomorphologies (Table 5). However, some geomorphology features were partially subcategorized using set depth ranges (Tamir et al., 2019). Also, the importance of depth in structuring community cover was evident when examining general trends in the GoA (Fig. 3) and globally (Kahng et al., 2010). The rocky peaks of some MR, MP, and LMSG features with topographic highs (Supplementary Fig. 1c) appeared elevated enough to avoid complete sediment burial and downslope transport often detrimental to MCE development (Sherman et al., 2010). However, LMSG features had lower average coral cover than MR and MP features, especially when factoring out sand, and instead had a higher coverage of Antipatharia. The deep depths associated with LMSG features could have limited hermatypic coral development compared to MR and MP features, although the latter two features still had <10% average coral cover when factoring out sand. Additionally, the association of coral rubble-forming *Alveopora* genera to UMT features (Supplementary Fig. 3c) may not have established for LMSG and LMT features (or adjacent MR and MP features) if this coral was unable to prosper at deeper depths.

Related to depth, additional examination of associations between geomorphology and coral composition may be connected to changing environmental conditions along the reef slope. Using a theoretical, process-based model of light as a single quantitative framework, Laverick et al. (2020) found shifts between distinct stony coral communities with depth (down to mesophotic reefs) throughout the world primarily resulted from varying light conditions along the reef slope. However, additional biological and environmental variables (e.g. aragonite saturation, temperature, hydrodynamic, and salinity) are expected to determine the community composition of different species and growth forms (Kleypas et al., 1999; Eyal et al., 2019; Turak and DeVantier, 2019; Kramer et al., 2020). As substrate type is a fundamental criterion for coral settlement selection and survival (Harrington et al., 2004), environmental process-based models (Kleypas et al., 1999; Laverick et al., 2020) combined with our study findings and additional analysis of environmental factors will offer a wider, improved understanding of MCE coral community spatial bathymetric distribution and habitat prediction.

Current study results highlight the explicit occupancy by coral depth-specialists at variable substrate conditions and geomorphologies, particularly on mesopohotic reefs (Eyal et al., 2016; Eyal-Shaham et al., 2016). The potential explanation for species-specific selective existence on different geomorphology types (see Supplementary Fig. 3) could clarify previous observations of particular species (e.g. *Alveopora* spp. and *Euphyllia paradivisa*) primary restrictions to specific depths and substrates (Eyal-Shaham et al., 2016; Eyal et al., 2016). At such a depth envelope, especially for MCEs, the difference between variable geomorphology features and associated habitats (e.g. sandy or rocky expanse), and suitable settlement substrate may favor the existent of specific species. The relative pervasiveness of *Leptoseris* identified in our study (Fig. 3d) mirrors others that indicate laminar (plate-like) coral growth forms, which are highly suitable for thriving in low-light conditions, dominate in mesophotic environments (Kahng et al., 2010; Kahng

Table 5
Comparisons between predictor variables and benthic (regular text) and lithologic (*italicized* text, after semicolon for BIOENV) balanced design datasets. The best combinations of predictor variables estimated by the BIOENV procedure that correlated with benthic and lithologic datasets are provided with rank correlation (ρ) for site and specific geomorphology (geomorph) similarity matrices. Distance-based linear model (DistLM) results for community composition variation, ordered from highest to lower proportion (Prop) of total variation explained. Summer K_dPAR calculated at 30 m depth (*KDS*), annual K_dPAR calculated at 30 m depth (*KDA*), Akaike information criterion (*AICc*).

BIOENV

Level	ρ (correlation)	Best variable(s)	p-value
Site	0.48;	Depth, BTM aspect;	0.001;
	0.35	*Depth, BTM aspect*	*0.020*
Geomorph.	0.48;	Depth, Slope;	0.029;
	0.47	*KDS*	*0.031*

DistLM

Variable	Dataset	AICc	Pseudo-F	Prop.	p-value
Depth	Benthic	225.50	16.20	0.35	0.001
KDA		225.38	2.41	0.05	0.066
Depth	*Lithologic*	*223.90*	*10.08*	*0.25*	*0.001*

et al., 2019). In the GoA, *Leptoseris* cover was greatest on MR, UMSG, and upper mesophotic shelf (UMS) features (unbalanced design, Supplementary Fig. 3d) and had low relative mean coral abundance (>15%) on shallower geomorphology features and on UMT features commonly dominated by rubble (based on the average cover of all pictures per site). *Leptoseris* can span the whole photic zone as seen throughout many Indo-Pacific reefs (Kahng et al., 2019), thriving with little light as a result of the optical geometry of their thin skeletons allowing for efficient light absorption while minimizing calcification (Kahng et al., 2020). While we acknowledge light is a primary factor controlling the species zonation along the depth gradient (Tamir et al., 2019), we suggest other factors play a role such as substrate type (e.g. immovable hard substrate versus loose rubble) related to geomorphology. Still, future settlement studies focusing on substrate contributions are needed to better constrain species zonation.

Besides depth, slope and K_dPAR were found to partially explain site benthic and lithologic composition based on geomorphology differences (Table 5; BIOENV), likely because these variables can impact how much light reaches the seafloor and potential sand burial (slope). Other tested variables provided little help explaining observed associations between geomorphology and surface community composition. Artifacts generated from multibeam data processing (Shaun Walbridge (ESRI), pers. com., 2019) often resulted in noisy raster creation using the BTM (Supplementary Fig. 1). This and available resolution likely prevented the association of distinct elevated features like MR and MP with higher relative rugosity and curvature differences from surrounding features (Supplementary Fig. 1). Alternatively, future examinations including more study sites and/or quantification of additional parameters (e.g. predation, competition, nutrient levels, water chemistry, sedimentation rates) may be needed to better detect and understand reasons for documented associations between surface community composition and geomorphology.

5.3. Formation history

A review of ancient mesophotic reef deposits and the limited studies inferring mesophotic accretion imply modern mesophotic reefs have some potential to create relief (Sherman et al., 2019). However, assuming carbonate production and environmental conditions were similar to the present since sea level has primarily stabilized (Shaked et al., 2002), modern benthic processes do not appear to provide an example for the structuring of northern GoA mesophotic geomorphology. First, our analysis found benthic and lithologic compositions distinctly different upon upper mesophotic terrace (UMT) and lower mesophotic terrace (LMT) features and similar upon UMT features and some adjacent upper mesophotic steep gradient (UMSG) and upper mesophotic shelf (UMS) features (Table 4). These results would be counterintuitive if the same processes were needed to create the upper and lower mesophotic terraces and if different processes were needed to distinguish UMT features from adjacent features. Second, although no samples were obtained, the underlying framework of rocky outcrop mesophotic ridge (MR) and mesophotic patch (MP) features appeared to consist of material different from the overlying biotic cover (e.g. SRO in Fig. 2). This suggests a non-modern age of feature formation. Additionally, despite relief above adjacent geomorphology features, modern coral carbonate production on MR and MP features was low, as evident by 2.2% and 0.4% average coral cover of all pictures, respectively (lithologic dataset), even when only considering non-sand categories (8.7% and 5.6% average coral cover of all pictures, respectively). This suggests limited modern carbonate/relief production. Horizontal linear extension rates in the GoA of *Leptoseris* (0.2–0.8 mm/yr; Fricke et al., 1987), the coral genera most commonly associated with MR features, and generally thin skeletal plate calcification (Kahng et al., 2020) would prevent accretion rates needed to create the recorded MR relief during the past ~6000 years that sea level has remained relatively stable (Shaked et al., 2002). Even if GoA *Leptoseris* grew as rapidly as on Hawaiian mesophotic reefs (Kahng et al., 2020), current abundances atop MR features could not have produced notable topographic relief in 6000 years. As such, it is unknown if some or all of these outcrops were originally built during the last ~6000 years at mesophotic depths by benthic organisms with different abundances than what is presently available. Still, ~6000 years may have provided ample time for syndepositional or subsequent bioerosion to produce or contribute to the unrecognizable substrate observed in drop-cam images. Alternatively, these formations may have partially formed earlier when sea level was lower (Grant et al., 2012).

Our study results provide formal identification of GoA UMT features, but we are unaware of formation timing estimates considering these features appear to only have been previously described as coral carpets (Hottinger, 2008). Bearing in mind the relative sea level curve (Grant et al., 2012), the most recent possible non-mesophotic UMT formation age is ~12–8 ka (Fig. 5a) as shore and beach facies and/or through erosional processes (e.g. white arrow in Fig. 5b), even when considering 10 m of potential vertical displacement (Makovsky et al., 2008). This possible accumulation may have been new or added to earlier terrace development when sea levels were near UMT depths (Fig. 5a). Terrace formation during the glacial to Holocene transition probably would not have supported coral reef development given the relatively high salinities that persisted in the region during the late glacial (Fenton et al., 2000).

Features similar to lower mesophotic terraces (LMTs) were previously inferred initiating <18 ka on a "100 m step" (Makovsky et al., 2008), ~21 ka as a submarine terrace system at depths of 90–110 m representing

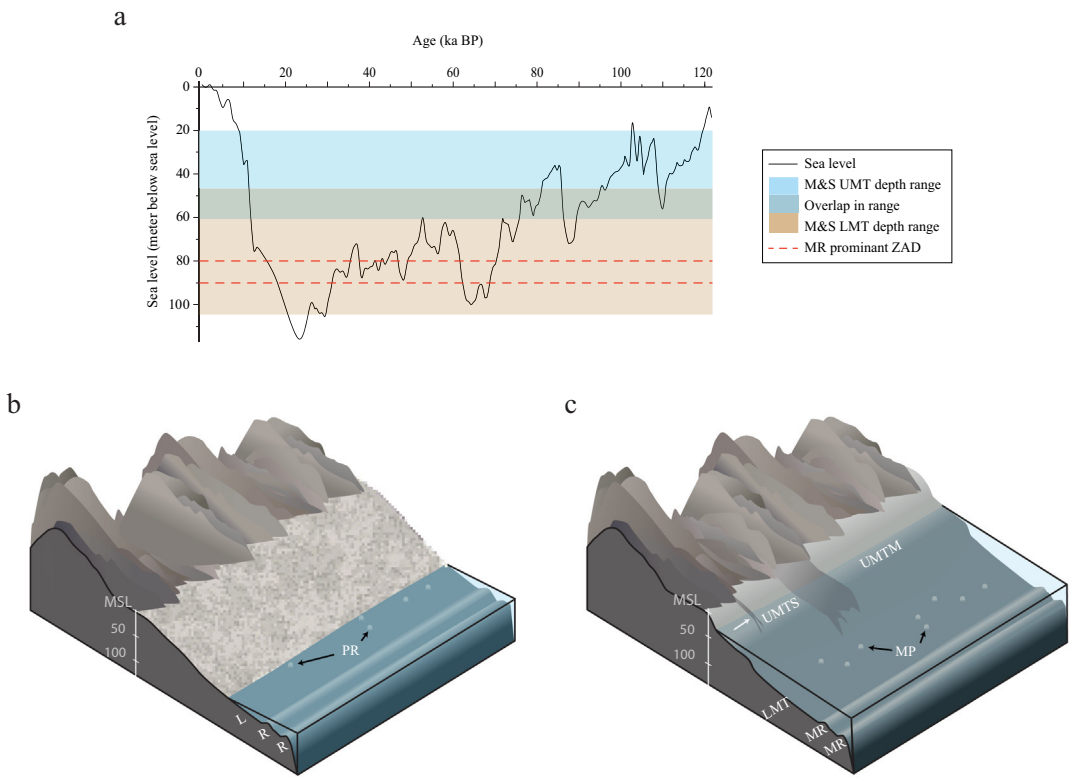

Fig. 5. Sea level and geomorphology feature development. (a) Sea level (Grant et al., 2012) compared to depths of newly defined northern GoA geomorphological features. Comparisons focus on upper mesophotic terrace (UMT), lower mesophotic terrace (LMT), and mesophotic ridge (MR) features. Depth ranges for terrace features, and depths of the two largest MR peak zonal area distributions (ZAD) (Fig. 1g) are displayed. Northern terrace features in the study area were not included due to potential movement along the Elat fault (Hartman et al., 2014); ranges displayed only represent the middle and southern (M&S) sections. (b) Potential LMT development relative to modern sea level (MSL) with a hypothesized lagoon (L), patch reefs (PR) now expressed as mesophotic patch features (MP), and a backstepped linear ridge and forereef system (R) now expressed as MR features. (c) Potential UMT development relative to MSL. The white arrow indicates possible erosion of the upper terrace feature (Fig. 1d) that could represent how the UMT feature currently appears discontinuous. The cartoon depicts UMT features in the southern (UMTS) and middle (UMTM) portions of the study area, as well as corresponding MP, MR, and LMT features. Cartoon depths in meters (m) not to scale.

former lowstand terraces or shorelines (Tibor et al., 2010), or 70–50 ka (Reches et al., 1987). Results from our study cannot provide further confirmation of these ages. We can only speculate that a long period of time was needed to create broad, continuous LMT features. The geomorphological orientation of GoA mesophotic ridges and patches bare similarities to shallow (near sea level), fringing or barrier reefs and backstepping retreat (e.g. Abbey et al., 2011) seaward of shallower juvenile patch reefs within a previous lagoon or low-relief backreef system (Fig. 5b). The proposed lagoon would now be buried under up to 5 m of sediment (Makovsky et al., 2008), which may also account for high sand cover over most of the MP and MR features except the most prominent topographic highs (e.g. Fig. 2c). This hypothesis implicates an ~70–30 ka range (including the range proposed by Reches et al., 1987) as the most recent possible non-mesophotic LMT, MR, and MP formation age. The 70–30 ka range preceded the high salinity Last Glacial Maximum (LGM) aplanktonic interval and superseded an earlier aplanktonic interval by a considerable amount of time in the northern Red Sea (Fenton et al., 2000). Numerous low-amplitude sea-level fluctuations (Fig. 5a) between 70 and 30 ka provided potentially suitable conditions to support coral reef development of antecedent MR and MP features near sea level (Fig. 5b). Still, possible bias with large classified terrace depth ranges and a lack of physically dated samples precludes precise identification of hypothesized initial geomorphology formation. As such, we emphasize the need to obtain substrate and cored subsurface samples from the mapped geomorphology features at mesophotic depths.

6. Conclusions

Determining geomorphological, lithological, and biological properties, and controls on reef distribution and biodiversity constitute key questions for better understanding and managing MCEs (Turner et al., 2019). Therefore, a comprehensive geomorphology map with 12 newly defined geomorphology features spanning mesophotic depths was created and still imagery was collected and analyzed, primarily over a range of mesophotic depths in the northern Gulf of Aqaba (GoA). These products provide a new tool to reef managers and researchers for identifying potential mesophotic reef distribution and baseline data. Eight distinct lithologic habitats, some with site median coral cover >50% at mesophotic depths, were found to reside on 10 of the newly defined geomorphology features. Lithologic and benthic cover distributions were found to be significantly different between geomorphology features. Depth was identified as a main tested variable to explain distinct relationships between community composition and geomorphology features, but improved bathymetry processing, additional sites, and examination of other variables are needed to better constrain associations. Modern processes could not provide a definite example of geomorphology development in the GoA. Alternatively, we suggest the most recent possible non-mesophotic depth marine initiation range was ~12–8 ka for newly identified upper mesophotic terrace features and ~70–30 ka for lower mesophotic terraces. However, a lack of substrate samples, potential classification bias, and a complex tectonic history prevents further speculation on feature formation timing and demonstrates the need for mesophotic reef coring. Still, identification of mesophotic ridge and patch geomorphology features and consideration of regional salinity history allows further speculation on lower mesophotic terrace formation (Fig. 5b). This speculation, along with imagery of lower mesophotic deposits, implies modern GoA lower mesophotic (60–150 m) reefs do not produce substantial carbonate deposits with vertical relief. However, the identification

and mapping of expansive, thick mesophotic coral rubble fields (Fig. 2b) and large (~1–2 m, vertical) coral-covered reef framework outcrops at depths of 40–60 m suggest mesophotic carbonate vertical accumulation may still be possible in the region and warrants direct sampling.

Declaration of competing interest

The authors declare that they have no known competing financial interests or personal relationships that could have appeared to influence the work reported in this paper.

Acknowledgements

This study was funded by a Zuckerman STEM Postdoctoral Scholarship (DKW). Partial support was provided by the Israel Science Foundation (ISF) No. 1191/16 (YL). GE received funding from the European Union's Horizon 2020 research and innovation program under the Marie Skłodowska-Curie grant agreement No. 796025. Multibeam data was provided by the Israel National Bathymetric Survey. The authors appreciate assistance from Emmanuel Sestieri (boat skipper), Ofir Hameiri (technical diving support), and other Interuniversity Institute for Marine Sciences (IUI) staff. Additional support was provided by Adi Ben Nun, Abraham Parrish, and Shaun Walbridge (ArcGIS), Renanel Pickholt (data and discussions), Gidon Winters (still images), Jessica Gordon (illustrations), Adi Zaken and Michelle Linklater (review), and the Israeli Nature and Parks Authority (fieldwork cooperation and MITgcm model simulations funds).

Appendix A. Supplementary data

Supplementary data associated with this article can be found in the online version, at https://doi.org/10.1016/j.geomorph.2020.107548. These data include the Google map of the 12 geomorphology features identified and described in this article.

References

Abbey, E., Webster, J.M., Beaman, R.J., 2011. Geomorphology of submerged reefs on the shelf edge of the Great Barrier Reef: the influence of oscillating Pleistocene Sea-levels. Mar. Geol. 288 (1), 61–78.

Al-Rifaiy, I., Cherif, O.H., 1988. The fossil coral reefs of al-Aqaba, Jordan. Facies. 18 (1), 219–229.

Beijbom, O., Edmunds, P.J., Kline, D.I., Mitchell, B.G., Kriegman, D., 2012. Automated annotation of coral reef survey images. IEEE Conference on Computer Vision and Pattern Recognition 2012, 1170–1177.

Ben-Avraham, Z., Almagor, G., Garfunkel, Z., 1979. Sediments and structure of the Gulf of Elat (Aqaba) - Northern Red Sea. Sediment. Geol. 23 (1), 239–267.

Berenshtein, I., Gildor, H., Fredj, E., Amitai, Y., Berman, H., Kiflawi, M., 2016. Israel Nature and Parks Authority report: Connectivity in the Gulf of Aqaba/Eilat, p., 22. http://dx.doi.org/10.13140/RG.2.2.17500.64643.

Bongaerts, P., Ridgway, T., Sampayo, E.M., Hoegh-Guldberg, O., 2010. Assessing the 'deep reef refugia' hypothesis: Focus on Caribbean reefs. Coral Reefs 29 (2), 309–327.

Bongaerts, P., Riginos, C., Brunner, R., Englebert, N., Smith, S.R., Hoegh-Guldberg, O., 2017. Deep reefs are not universal refuges: Reseeding potential varies among coral species. Sci. Adv. 3 (2), E1602373.

Braithwaite, C.J.R., 1987. Geology and palaeogeography of the Red Sea region. In: Edwards, A.J., Head, S.M. (Eds.), Key Environments-Red Sea. Pergamon Press, Oxford, pp. 22–44.

Bridge, T., Beaman, R., Done, T., Webster, J., 2012. Predicting the location and spatial extent of submerged coral reef habitat in the Great Barrier Reef World Heritage Area, Australia. PLoS One 7 (10), e48203.

Bridge, T.C.L., Done, T.J., Beaman, R.J., Friedman, A., Williams, S.B., Pizarro, O., Webster, J.M., 2011. Topography, substratum and benthic macrofaunal relationships on a tropical mesophotic shelf margin, central Great Barrier Reef. Australia. Coral Reefs. 30, 143–153.

Cacciapaglia, C., van Woesik, R., 2015. Reef-coral refugia in a rapidly changing ocean. Glob. Chang. Biol. 21 (6), 2272–2282.

Clarke, K.R., Ainsworth, M., 1993. A method of linking multivariate community structure to environmental variables. Mar. Ecol. Prog. Ser. 92, 205–219.

Clarke, K.R., Gorley, R.N., 2015. PRIMER v7: User Manual/Tutorial. PRIMER-E, Plymouth, p. 296.

Core Team, R., 2020. R: A Language and Environment for Statistical Computing. Anonymous. R Foundation for Statistical Computing, Vienna, Austria. URL, In https://www.R-project.org/.

Costa, B., Kendall, M.S., Parrish, F.A., Rooney, J., Boland, R.C., Chow, M., Lecky, J., Montgomery, A., Spalding, H., 2015. Identifying suitable locations for mesophotic hard corals offshore of Maui, Hawai'i. PLoS One 10 (7), e0130285.

Dullo, W., Reijmer, J.J.G., Schuhmacher, H., Eisenhauer, A., Hassan, M., Heiss, G.A., 1996. Holocene reef growth and recent carbonate production in the Red Sea. In: Reijmer, J.J.G., Neuweiler, F., Gunkel, F. (Eds.), Global and Regional Controls on Biogenic Sedimentation. I. Reef evolution. Research reports. Göttinger Arbeiten zur Geologie und Paläontologie, Göttingen, pp. 13–17.

Eyal, G., Eyal-Shaham, L., Cohen, I., Tamir, R., Ben-Zvi, O., Sinniger, F., Loya, Y., 2016. *Euphyllia paradivisa*, a successful mesophotic coral in the northern Gulf of Eilat/Aqaba, Red Sea. Coral Reefs 35 (1), 91–102.

Eyal, G., Tamir, R., Kramer, N., Eyal-Shaham, L., Loya, Y., 2019. The Red Sea: Israel. In: Loya, Y., Puglise, K.A., Bridge, T.C.L. (Eds.), Mesophotic Coral Ecosystems. Coral Reefs of the World vol. 12. Springer, Cham, pp. 199–214.

Eyal-Shaham, L., Eyal, G., Tamir, R., Loya, Y., 2016. Reproduction, abundance and survivorship of two *Alveopora* spp. in the mesophotic reefs of Eilat, Red Sea. Sci Rep. 6, 20964.

Fenton, M., Geiselhart, S., Rohling, E.J., Hemleben, C., 2000. Aplanktonic zones in the Red Sea. Mar. Micropaleontol. 40 (3), 277–294.

Fine, M., Gildor, H., Genin, A., 2013. A coral reef refuge in the Red Sea. Glob. Chang. Biol. 19 (12), 3640–3647.

Fine, M., Cinar, M., Voolstra, C.R., Safa, A., Rinkevich, B., Laffoley, D., Hilmi, N., Allemand, D., 2019. Coral reefs of the Red Sea — challenges and potential solutions. Reg. Stud. Mar. Sci. 25, 100498.

Frade, P.R., Bongaerts, P., Englebert, N., Rogers, A., Gonzalez-Rivero, M., Hoegh-Guldberg, O., 2018. Deep reefs of the Great Barrier Reef offer limited thermal refuge during mass coral bleaching. Nat. Commun. 9 (1), 3447.

Fricke, H.W., Vareschi, E., Schlichter, D., 1987. Photoecology of the coral *Leptoseris fragilis* in the Red Sea twilight zone (an experimental study by submersible). Oecologia. 73 (3), 371–381.

Grant, K.M., Rohling, E.J., Bar-Matthews, M., Ayalon, A., Medina-Elizalde, M., Bronk Ramsey, C., Satow, C., Roberts, A.P., 2012. Rapid coupling between ice volume and polar temperature over the past 150,000 years. Nature 491, 744–747. https://doi.org/10.1038/nature11593.

Harrington, L., Fabricius, K., De'ath, G., Negri, A., 2004. Recognition and selection of settlement substrata determine post-settlement survival in corals. Ecology. 85 (12), 3428–3437.

Hartman, G., Niemi, T.M., Tibor, G., Ben-Avraham, Z., Al-Zoubi, A., Makovsky, Y., Akawwi, E., Abueladas, A., Al-Ruzouq, R., 2014. Quaternary tectonic evolution of the Northern Gulf of Elat/Aqaba along the Dead Sea Transform. J. Geophys. Res. Solid Earth 119 (12), 9183–9205.

Hinderstein, L.M., Marr, J.C.A., Martinez, F.A., Dowgiallo, M.J., Puglise, K.A., Pyle, R.L., Zawada, D.G., Appeldoorn, R., 2010. Theme section on "Mesophotic Coral Ecosystems: Characterization, Ecology, and Management". Coral Reefs 29 (2), 247–251.

Hottinger, L., 2008. The role of biogenous carbonate production in the ecology of shallow benthic communities in oligotrophic waterbodies. In: Por, F.D. (Ed.), Aqaba-Eilat, the Improbable Gulf: Environment, Biodiversity and Preservation. Magnes Press, Jerusalem, pp. 153–176.

Hughes, T.P., Anderson, K.D., Connolly, S.R., Heron, S.F., Kerry, J.T., Lough, J.M., Baird, A.H., Baum, J.K., Berumen, M.L., Bridge, T.C., Claar, D.C., Eakin, C.M., Gilmour, J.P., Graham, N.A.J., Harrison, H., Hobbs, J.A., Hoey, A.S., Hoogenboom, M., Lowe, R.J., McCulloch, M.T., Pandolfi, J.M., Pratchett, M., Schoepf, V., Torda, G., Wilson, S.K., 2018. Spatial and temporal patterns of mass bleaching of corals in the Anthropocene. Science. 359 (6371), 80–83.

International Hydrographic Organization (IHO), 2013. Standardization of Undersea Feature Names: Guidelines, Proposal Form, Terminology, Publication B-6. International Hydrographic Organisation, Monaco.

Kahng, S.E., Garcia-sais, J.R., Spalding, H.L., Brokovich, E., Wagner, D., Weil, E., Hinderstein, L., Toonen, R.J., 2010. Community ecology of mesophotic coral reef ecosystems. Coral Reefs 29 (2), 255–275.

Kahng, S.E., Akkaynak, D., Shlesinger, T., Hochberg, E.J., Wiedenmann, J., Tamir, R., Tchernov, D., 2019. Light, temperature, photosynthesis, heterotrophy, and the lower depth limits of mesophotic coral ecosystems. In: Loya, Y., Puglise, K.A., Bridge, T.C.L. (Eds.), Mesophotic Coral Ecosystems. Coral Reefs of the World vol. 12. Springer, Cham, pp. 801–828.

Kahng, S.E., Watanabe, T.K., Hu, H., Watanabe, T., Shen, C., 2020. Moderate zooxanthellate coral growth rates in the lower photic zone. Coral Reefs 39, 1273–1284. https://doi.org/10.1007/s00338-020-01960-4.

Klein, R., Loya, Y., Gvirtzman, G., Isdale, P.J., Susic, M., 1990. Seasonal rainfall in the Sinai Desert during the late Quaternary inferred from fluorescent bands in fossil corals. Nature. 345 (6271), 145–147.

Kleypas, J.A., McManus, J.W., Meñez, L.A.B., 1999. Environmental limits to coral reef development: where do we draw the line? Amer. Zool. 39 (1), 146–159.

Kramer, N., Tamir, R., Eyal, G., Loya, Y., 2020. Coral morphology portrays the spatial distribution and population size-structure along a 5–100 m depth gradient. Front. Mar. Sci. 7, 615.

Laverick, J.H., Tamir, R., Eyal, G., Loya, Y., 2020. A generalized light-driven model of community transitions along coral reef depth gradients. Glob. Ecol. Biogeogr. 29, 1554–1564. https://doi.org/10.1111/geb.13140.

Lesser, M.P., Slattery, M., 2011. Phase shift to algal dominated communities at mesophotic depths associated with lionfish (*Pterois volitans*) invasion on a Bahamian coral reef. Biol.Invasions. 13 (8), 1855–1868.

Lesser, M.P., Slattery, M., Leichter, J.J., 2009. Ecology of mesophotic coral reefs. J. Exp. Mar. Biol. Ecol. 375 (1–2), 1–8.

Linklater, M., Carroll, A.G., Hamylton, S.M., Jordan, A.R., Brooke, B.P., Nichol, S.L., Woodroffe, C.D., 2016. High coral cover on a mesophotic, subtropical island platform at the limits of coral reef growth. Cont. Shelf Res. 130, 34–46.

Loya, Y., 1972. Community structure and species diversity of hermatypic corals at Eilat, Red Sea. Mar. Biol. 13 (2), 100–123.
Loya, Y., Eyal, G., Treibitz, T., Lesser, M.P., Appeldoorn, R., 2016. Theme section on mesophotic coral ecosystems: advances in knowledge and future perspectives. Coral Reefs 35 (1), 1–9.
Mesophotic Coral Ecosystems. In: Loya, Y., Puglise, K.A., Bridge, T.C.L. (Eds.), Coral Reefs of the World (Volume 12). Publishing, Springer International.
Lundblad, E.R., Wright, D.J., Miller, J., Larkin, E.M., Rinehart, R., Naar, D.F., Donahue, B.T., Anderson, S.M., Battista, T., 2006. A benthic terrain classification scheme for American Samoa. Mar. Geod. 29 (2), 89–111.
Makovsky, Y., Wunch, A., Ariely, R., Shaked, Y., Rivlin, A., Shemesh, A., Ben Avraham, Z., Agnon, A., 2008. Quaternary transform kinematics constrained by sequence stratigraphy and submerged coastline features: the Gulf of Aqaba. Earth Planet. Sci. Lett. 271 (1–4), 109–122.
Marshall, J., Adcroft, A., Hill, C., Perelman, L., Heisey, C., 1997. A finite-volume, incompressible Navier Stokes model for studies of the ocean on parallel computers. J. Geophys. Res. 102, 5753–5766.
Muir, P.R., Pichon, M., 2019. Biodiversity of reef-building, scleractinian corals. In: Loya, Y., Puglise, K.A., Bridge, T.C.L. (Eds.), Mesophotic Coral Ecosystems. Coral Reefs of the World vol. 12. Springer, Cham, pp. 589–620.
Muir, P.R., Wallace, C.C., Done, T., Aguirre, J.D., 2015. Limited scope for latitudinal extension of reef corals. Science. 348 (6239), 1135–1138.
Oksanen, J., Blanchet, F.G., Friendly, M., Kindt, R., Legendre, P., McGlinn, D., Minchin, P.R., O'Hara, R.B., Simpson, G.L., Solymos, P., Stevens, M.H.H., Szoecs, E., Wagner, H., 2018. Vegan: Community Ecology Package. R package version 2, 4–6.
Pandolfi, J.M., Bradbury, R.H., Sala, E., Hughes, T.P., Bjorndal, K.A., Cooke, R.G., McArdle, D., McClenachan, L., Newman, M.J.H., Paredes, G., Warner, R.R., Jackson, J.B.C., 2003. Global trajectories of the long-term decline of coral reef ecosystems. Science. 301 (5635), 955.
Purkis, S.J., Rowlands, G.P., Riegl, B.M., Renaud, P.G., 2010. The paradox of tropical karst morphology in the coral reefs of the arid Middle East. Geology. 38 (3), 227–230.
Reches, Z., Erez, J., Garfunkel, Z., 1987. Sedimentary and tectonic features in the northwestern Gulf of Elat, Israel. Tectonophysics. 141 (1–3), 169–180.
Riegl, B., Piller, W.E., 2003. Possible refugia for reefs in times of environmental stress. Int. J. Earth Sci. 92 (4), 520–531.
Rocha, L.A., Pinheiro, H.T., Shepherd, B., Papastamatiou, Y.P., Luiz, O.J., Pyle, R.L., Bongaerts, P., 2018. Mesophotic coral ecosystems are threatened and ecologically distinct from shallow water reefs. Science. 361 (6399), 281.
Sade, A., Hall, J.K., Tibor, G., Niemi, T.M., Ben-Avraham, Z., Al-Zoubi, A.S., Hartman, G., Akawwi, E., Abueladas, A., Amit, G., 2008. The Israel National Bathymetric Survey: Northern Gulf of 'Aqaba/Elat Poster. Isr. J. Earth Sci. 57, 139–144.
Shaked, Y., Marco, S., Lazar, B., Stein, M., Cohen, C., Sass, E., Agnon, A., 2002. Late Holocene shorelines at the Gulf of Aqaba: migrating shorelines under conditions of tectonic and sea level stability. EGU Stephan Mueller Special Publication Series 2, 105–111.
Shaked, Y., Lazar, B., Marco, S., Stein, M., Agnon, A., 2011. Late Holocene events that shaped the shoreline at the northern Gulf of Aqaba recorded by a buried fossil reef. Isr. J. Earth Sci. 58, 355–368.
Sherman, C., Nemeth, M., Ruíz, H., Bejarano, I., Appeldoorn, R., Pagán, F., Schärer, M., Weil, E., 2010. Geomorphology and benthic cover of mesophotic coral ecosystems of the upper insular slope of Southwest Puerto Rico. Coral Reefs 29 (2), 347–360.
Sherman, C.E., Locker, S.D., Webster, J.M., Weinstein, D.K., 2019. Geology and geomorphology. In: Loya, Y., Puglise, K.A., Bridge, T.C.L. (Eds.), Mesophotic Coral Ecosystems. Coral Reefs of the World vol. 12. Springer, Cham, pp. 849–878.
Shlesinger, T., Grinblat, M., Rapuano, H., Amit, T., Loya, Y., 2018. Can mesophotic reefs replenish shallow reefs? Reduced coral reproductive performance casts a doubt. Ecology. 99 (2), 421–437.
Suka, R., Rooney, J., 2017. Acoustic Characterization of Mesophotic Coral Reef Ecosystems of West Hawaii U.S. Dep. Commer. NOAA Tech. Memo., NOAA-TMNMFS- PIFSC 61, 31. https://doi.org/10.7289/V5/TM-PIFSC-61.
Tamir, R., Eyal, G., Kramer, N., Laverick, J.H., Loya, Y., 2019. Light environment drives the shallow-to-mesophotic coral community transition. Ecosphere. 10 (9), e02839. https://doi.org/10.1002/ecs2.2839.
Tibor, G., Niemi, T.M., Ben-Avraham, Z., Al-Zoubi, A., Sade, R.A., Hall, J.K., Hartman, G., Akawi, E., Abueladas, A., Al-Ruzouq, R., 2010. Active tectonic morphology and submarine deformation of the northern Gulf of Eilat/Aqaba from analyses of multibeam data. Geo-Mar. Lett. 30 (6), 561–573.
Turak, E., DeVantier, L., 2019. Reef-building corals of the upper mesophotic zone of the central Indo-West Pacific. In: Loya, Y., Puglise, K., Bridge, T.C.L. (Eds.), Mesophotic Coral Ecosystems. Coral Reefs of the World vol. 12. Springer, Cham, pp. 621–651.
Turner, J.A., Babcock, R.C., Hovey, R., Kendrick, G.A., 2017. Deep thinking: a systematic review of mesophotic coral ecosystems. ICES J Mar Sci. fsx085.
Turner, J.A., Andradi-Brown, D., Gori, A., Bongaerts, P., Burdett, H.L., Ferrier-Pagès, C., Voolstra, C.R., Weinstein, D.K., Bridge, T.C.L., Costantini, F., Gress, E., Laverick, J., Loya, Y., Goodbody-Gringley, G., Rossi, S., Taylor, M.L., Viladrich, N., Voss, J.D., Williams, J., Woodall, L.C., Eyal, G., 2019. Key questions for research and conservation of mesophotic coral ecosystems and temperate mesophotic ecosystems. In: Loya, Y., Puglise, K.A., Bridge, T.C.L. (Eds.), Mesophotic Coral Ecosystems. Coral Reefs of the World 12. Springer, Cham, pp. 989–1003.
Walbridge, S., Slocum, N., Pobuda, M., Wright, J.D., 2018. Unified geomorphological analysis workflows with Benthic Terrain Modeler. Geosciences. 8 (3), 24.
White, K.N., Weinstein, D.K., Ohara, T., Denis, V., Montenegro, J., Reimer, J.D., 2017. Shifting communities after typhoon damage on an upper mesophotic reef in Okinawa. Japan. PeerJ. 5, e3573.
Winters, G., Edelist, D., Shem-Tov, R., Beer, S., Rilov, G., 2017. A low cost field-survey method for mapping seagrasses and their potential threats: an example from the northern Gulf of Aqaba, Red Sea. Aquatic Conserv: Mar Freshw Ecosyst 27 (2), 324–339.